Schweizerische Eidgenossenschaft
Confédération suisse
Confederazione Svizzera
Confederaziun svizra

Department of the Environment, Transport, Energy and Communication DETEC

Swiss Federal Office of Energy SFOE
Energy Research

2021

Scale-up of a Microbial Fuel Cell

Final Report

Date: 25.01.2021
Town: Sion

Publisher:
Swiss Federal Office of Energy SFOE
Biomass
CH-3003 Bern
www.bfe.admin.ch

Agent:
HES-SO Valais-Wallis
Route du Rawyl 64, CH-1950 Sion
www.hevs.ch

Authors:
Ing. Maxime Blatter, HES-SO Valais-Wallis, maxime.blatter@hevs.ch
Prof. Dr. Fabian Fischer, HES-SO Valais-Wallis, fabian.fischer@hevs.ch

SFOE head of domain: Dr. Sandra Hermle
SFOE programme manager: Dr. Sandra Hermle
SFOE contract number: SI/501573-01

Swiss Federal Office of Energy SFOE
Mühlestrasse 4, CH-3063 Ittigen; postal address: CH-3003 Bern
Phone +41 58 462 56 11 · Fax +41 58 463 25 00 · contact@bfe.admin.ch · www.bfe.admin.ch

1 Abstract

This comprhesive projet report shows in essence a more than yearlong uninterrupted MFC-reactor use under realistic operating conditions. The utilisation of a pilot microbial fuel cell (MFC) of ~1 m^3 capacity was researched to assess the possible implementation of large-scale MFC-technologies in wastewater treatment plants (WWTPs). The purpose of the project was to examine how to lower wastewater cleaning costs, in comparison to traditional biological treatments, while generating and storing energy.

As an initial investigation, prototype based-experiments (annual report 2018) were performed to define determinant values of bioelectrochemical parameters (potential, current and internal resistance) and estimate the final output of the scale-up system in terms of power and energy production. The prototype allowed selecting best suitable material for the implementation of the scale-up MFC installation.

The 1000-L MFC was directly implemented in *Châteauneuf* (*Valais*, *Switzerland*) municipal WWTP, where it was operated with influents from a primary clarifier, either in batch or continuous mode (up to 1 m^3/day). After an acclimatation period of 4 months, the 1000-L MFC was operated in an uninterrupted manner using energy storing modules. The electricity generation was monitored with the help of an embedded-computed system that allowed to independently monitor working potentials and currents of each MFC unit of the scale-up MFC (64 cells in total). Key operating parameters such as anolyte and catholyte flow as well as oxygenation rates were adapted to maximize the systems performance. The energy recovery was optimised by maximum power point tracking (MPPT) devices and stored on lithium batteries, subsequently employed to recharge smartphones as an example application. The wastewater purification effect was controlled over chemical oxygen demand (COD) removal and the end process values corresponded well with the limits required by Swiss legislation. Comparatively with aerobic biological lagoons, energy might be saved by decreasing the air (O_2) supply to the microbiome (using alternative oxygenated water source, algae or air-cathodes). The system performance evolved with biofilm maturation (a microorganism selection occurred within the reactor and specific exoelectrogen bacteria such as *Geobacter* developed) and was also affected by weather conditions as well as human activity. Process optimisation is possible by addressing the voltage reversal causes and limiting electron sinks (presence of residual oxygen, denitrification, sulphate / sulphite reduction, methane production, biomass formation and metals reduction). The energy density and efficiency were comparable with published data for smaller installations (> 10 L). Denitrification and micropollutant elimination were observed. No heavy metal were detected and elements such as calcium, potassium, sodium and sulphur were partly removed from wastewater.

The 1000-L MFC fulfilled so far the needs of this pilot investigation and future industrial scale became an option due to the beneficial effects of the MFC technology applied as it treated wastewater well.

Table of Content:

1.1 MFC Technology

MFCs are bioelectrochemical devices permitting spontaneous generation of electrical currents. A cell is composed of two distinct compartments (*Fig.2*): an anodic chamber where the microorganisms degrade the organic matter by oxidation and a cathodic chamber where the soluble oxygen (final electron acceptor) is reduced into water. The two compartments are separated by a cation exchange membrane (*VANADion™*). The MFC working principle applied to WWTP is simple. Wastewater is used within the anodic compartment of the cell (*Fig.2*). Wastewater naturally contains organic matter and a multitude of different microorganisms, which grow and form a biofilm on the anodic surface. During the metabolism of these organisms, the organic matter is degraded and converted to protons (H^+), electrons (e^-), carbon dioxide (CO_2) and biomass. During the oxidation, electrons are directly transferred to the anode from the biofilm. The electrons travel, then, to the cathodic compartment through an external circuit and react with the soluble oxygen contained at the cathode to produce water (*Eq.1*)

$$1/2\, O_2 + 2e^- + 2H^+ \rightarrow H_2O \qquad (1)$$

When the circuit is closed with an external load, an electrical current is produced depending on the external resistance. In order to respect the electro-neutrality of the cell, positively charged particles migrate through the membrane from anodic to cathodic compartment (*Fig.2*).

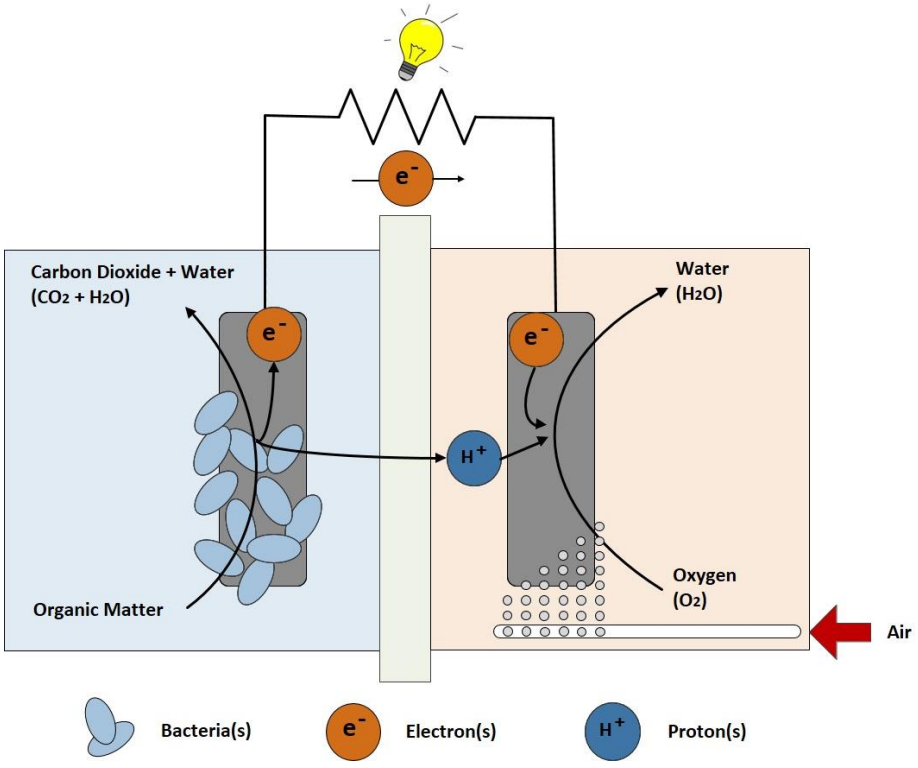

Figure 1: *Microbial fuel cell (MFC) with an anode covered by a biofilm of microorganisms and a cathode used for oxygen reduction. A cation exchange membrane separates the two half-cells.*

MFC is a promising technology to produce clean and sustainable energy. In fact, it allows spontaneous (thermodynamic favourable [19-21]) substrate conversion into electrical energy under close to neutral pH at ambient temperature. A range of inexpensive sources of organic matter can be used in the anodic compartment. By removing the organic matter present in wastewater, MFCs are envisaged in wastewater treatment where organic compounds are the main pollutants. In addition to organic matter oxidation, a denitrification process occurs, reducing soluble N-species present in wastewater into nitrogen gas. Moreover, in MFCs the microorganisms respire over electrodes and do not need aerobic conditions to function, indicating that wastewater treatment costs should be lower than traditional biological treatments.

1.2 Research Purpose and Scope

A 1000-L MFC installation was designed and assembled by the *HES-SO Valais-Wallis* and directly implemented on the WWTP of *Châteauneuf* (City of *Sion*). The main goal of the project was to treat wastewater at a fraction of the cost of a traditional biological lagoon, while generating and storing energy (*Fig.3*). Two common resources were needed to operate the MFC: wastewater charged with organic matter and microorganisms (anolyte) as well as aerated groundwater (catholyte). The system outputs were electricity and treated wastewater. The energy recovery was optimized by maximum power point tracking (MPPT) devices and stored on lithium batteries. Denitrification, methane generation and cations recuperation were other aspects investigated in the study.

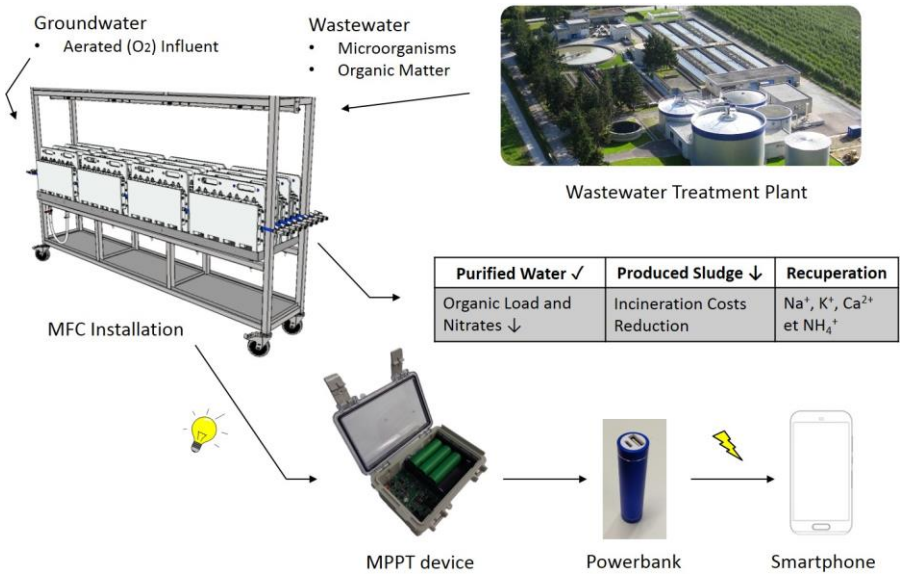

Figure 2: *MFC installation implemented in Châteauneuf WWTP. Wastewater issued from the primary clarifier was used as anolyte and aerated groundwater as catholyte. The 1000-L MFC produced*

electricity, which was reused here to recharge a smartphone for demonstration purposes. The wastewater was treated with several additional advantages such as denitrification and sludge reduction.

The large scale MFC was used as a pilot to determine if a potential industrialisation was feasible and applicable with currently available technology in a foreseeable future. The present study aimed to clarify the benefits of such an installation by answering the following questions:

1. What is the energy saving potential regarding oxygen / air supply (consumption) in comparison to traditional biological lagoon treatment? Which potential energy savings solutions are conceivable?
2. What is the process effectiveness of the MFC installation in terms of current (*Coulombic efficiency*) and energy (*Energy efficiency*)? How much energy is recoverable per cubic meter of treatable wastewater? Does the system performances increase over time?
3. What is the level of wastewater purification achievable with such a system? Are the limitations for COD removal present in the Swiss legislation fulfilled? What is the treating capacity of the system in terms of flow rates?
4. Could the wastewater of the 1000-L MFC be released into the environment? What are the concentrations of phosphate (PO_4^{3-}) and heavy metals in effluents? What happens to $FeCl_3$? Is it reduced?
5. Is there any denitrification with the proposed MFC system? Could the installation address the micropollutants problematic ? At what yield ?
6. Which elements could be recovered from the process? Could ammonium (NH_4^+), calcium (Ca^{2+}) sodium (Na^+) and potassium (K^+) be collected? In what quantities?
7. What are the microorganisms' consortia involved in the MFC scale-up installation? Are they different from the ones present in biological treatment?
8. Are there sinks of electrons observed implementing the MFC technology? Where the electrons, which do not end up as electricity, disappear? Is there a possible methane (CH_4) production with the proposed system?

Once all questions will be addressed, a feasibility and economic analysis is performed to examine a possible industrial implementation.

2 Material and Methods

2.1 Microbial Fuel Cell Construction and Installation

The 1000-L MFC was constructed in the polymechanic shop of *HES-SO Valais-Wallis* and assembled in the WWTP of *Châteauneuf*. The 1000-L MFC consisted of 64 identical MFC units (*Fig.4*) made of polyethylene terephthalate glycol-modified (PETG). Each cells size was 67.0 x 46.4 x 14.1 cm, for a total electrolyte volume up to 16.25 L. A VANADion™ membrane (*Ion Power*) was used to separate the two half-cells into compartments of the same volume. Eight reticulated vitreous carbon (RVC, *ERG Aerospace Corporation*) electrodes (21.0 x 13.0 x 3.0 cm) were used, four in each chamber.

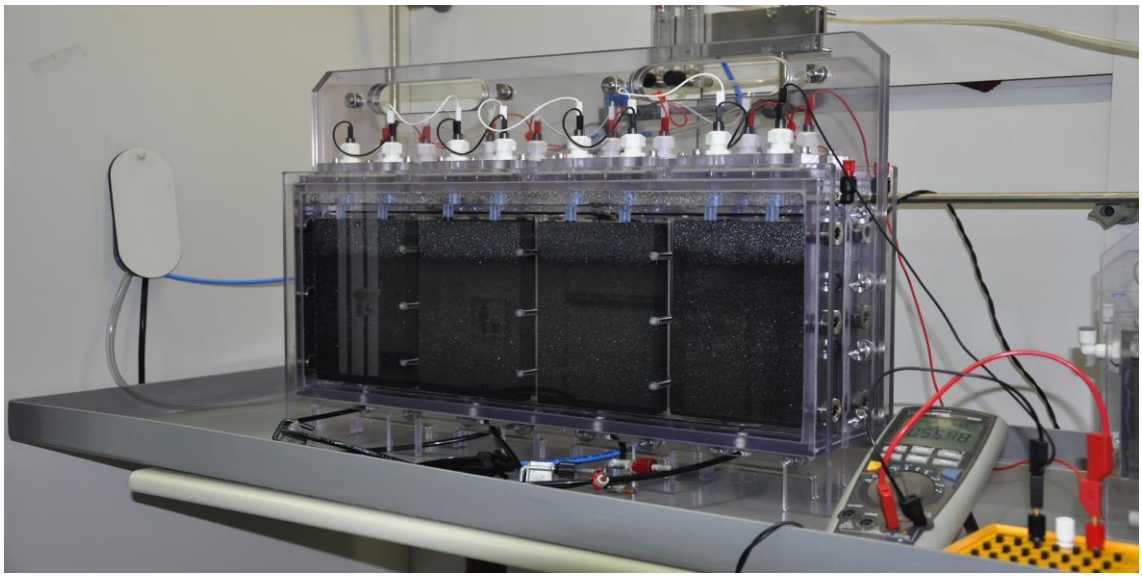

Figure 3: *Microbial fuel cell prototype used to determine key bioelectrochemical parameters.*

The complete installation had a minimal working volume of 928 L. At full capacity, the system accommodated a maximal volume of 1.03 m^3. The 64 MFCs were organized into 4 groups of 16 units and placed on 4 separated carts (*Fig.5-6*). Each reactor unit had two inputs and outputs for water (catholyte) and wastewater (anolyte) circulation. The cells were hydraulically interconnected (4 lines per cart) by polyurethane (PU) tubing (11 mm internal diameter (ID), *Legris*) of 10.3 cm. The same tubing (14.8 cm) connected the reactors between the four carts. Two 4-channel peristaltic pumps with adjustable flow rates (BT100S-1, *Golander Pump*) were employed to supply water and wastewater to the 1000 L-MFC. The water in the anode was pumped from a groundwater source, whereas wastewater was from the primary clarifier of the WWTP. Airflow tubings (polyamide (PA), 4 mm ID, *Legris*) were connected to the cathodic compartment of each cell to enrich the catholyte in dissolved O_2. A 1.6-bar manometer was employed for air pressure regulation. The electrical connections (*Stäubli*) were independent from one cart (16 MFCs) to the other. On the same cart, 4-linear units were connected in parallel and these 4-line stacks were wired serially (*Sec. 3.3*), branched with an external resistance (R-

Box 01 Resistor Decade Box, *Voltcraft*) and multimeter (VC-960 digital multimeter, *Voltcraft Plus*). The determination of soluble O_2 concentration was performed using a dissolve oxygen probe (HI2040 edge, *Hanna instruments*), which was also employed to measure electrolyte temperatures. The pH was monitored with the help of a pH meter (827 pH lab, *Metrohm*).

Figure 4: *1000-L MFC with 64 reactor units assembled on 4 carts as stacks. Water and wastewater were introduced from one side (right), passing through 16 MFC-units before reaching the outlet at the other side of the system (outer left). Air flow tubes were branched to the cathodic compartment of each cell. Resistance box and multimeter were connected for electrical parameters determination.*

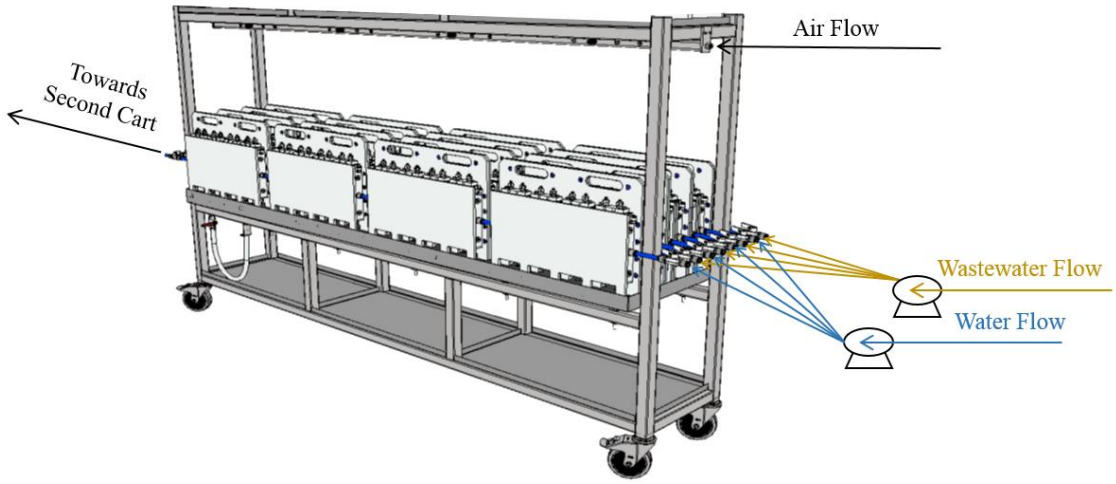

Figure 5: *Details of one single cart with 16 MFC-units. The inlets (2x4) were connected to two 4-channel peristaltic pumps to supply the system with groundwater (catholyte) and wastewater (anolyte). An air flow tube was employed to supply air in each half-cell to increase the O_2 concentration in the catholyte. The cells of each cart were connected between themselves by polyurethane tubing.*

2.2 Monitoring Cards & MPPT Devices

To observe the current (I $[A]$) and potential (U $[V]$) of each MFC, 64 monitoring cards (*Fig.7A*) were designed and manufactured by the Embedded-Computing Systems (ECS) Institute HE-Arc of *St-Imier* (*Bern, Switzerland*). Those cards were controlled by a Raspberry Pi connected to a central computer for data acquisition. The power and energy generated (*Eq.2*) were calculated from these data. Moreover, the monitoring cards allowed disconnecting individual cells from the electrical circuit if the cell potential was inferior to a defined set value (25 mV), to prevent voltage reversal. The electricity generation was optimized with maximum power point tracking devices (ECS Institute of *St-Imier*) and stored to four sets of lithium batteries. These four storage modules (*Fig.7B*) were equally connected to a Raspberry Pi linked to the same computer.

$$E = \int_0^t P\,dt = \int_0^t U\,I\,dt \qquad (2)$$

E $[Wh]$: the energy generated by the MFC, P $[W]$: the power produced, U $[V]$: the potential of the cell, I $[A]$: the current passing through the system and t $[h]$: the process duration. The electrical energy produced by the entire system was calculated by summing the energy generated by each individual cell.

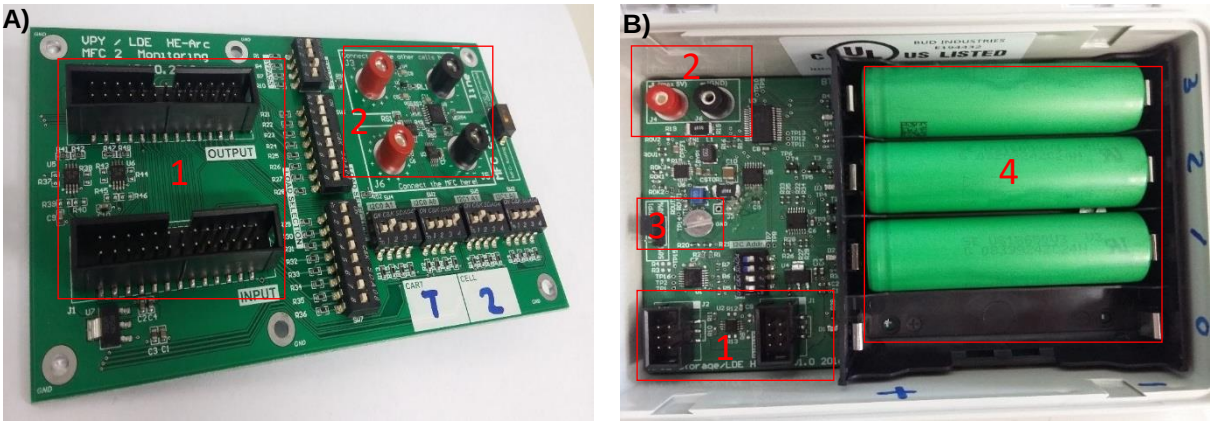

Figure 6: ***A****) Monitoring card permitting to follow the current and potential of each MFC unit. All monitoring cards were connected to one Raspberry pi (****1****) for data acquisition. The cards were branched to the cells and to each other by using four 2 mm connection plugs (****2****).* ***B****) Energy storage module including a MPPT device (****3****) to maximize the system output in terms of power. Four batteries can be separately charged (****4****).*

Additional pictures can be seen in the appendix section (*Sec. 8.2B*)

2.3 Electrical Configuration

The electrical circuits and other devices were independent from one cart to the other due to the fact that each cart possessed its own storage module. There was no electrical connection between the four carts of the 1000-L MFC installation. However, the configuration was identical for all of them (*Fig.8*):

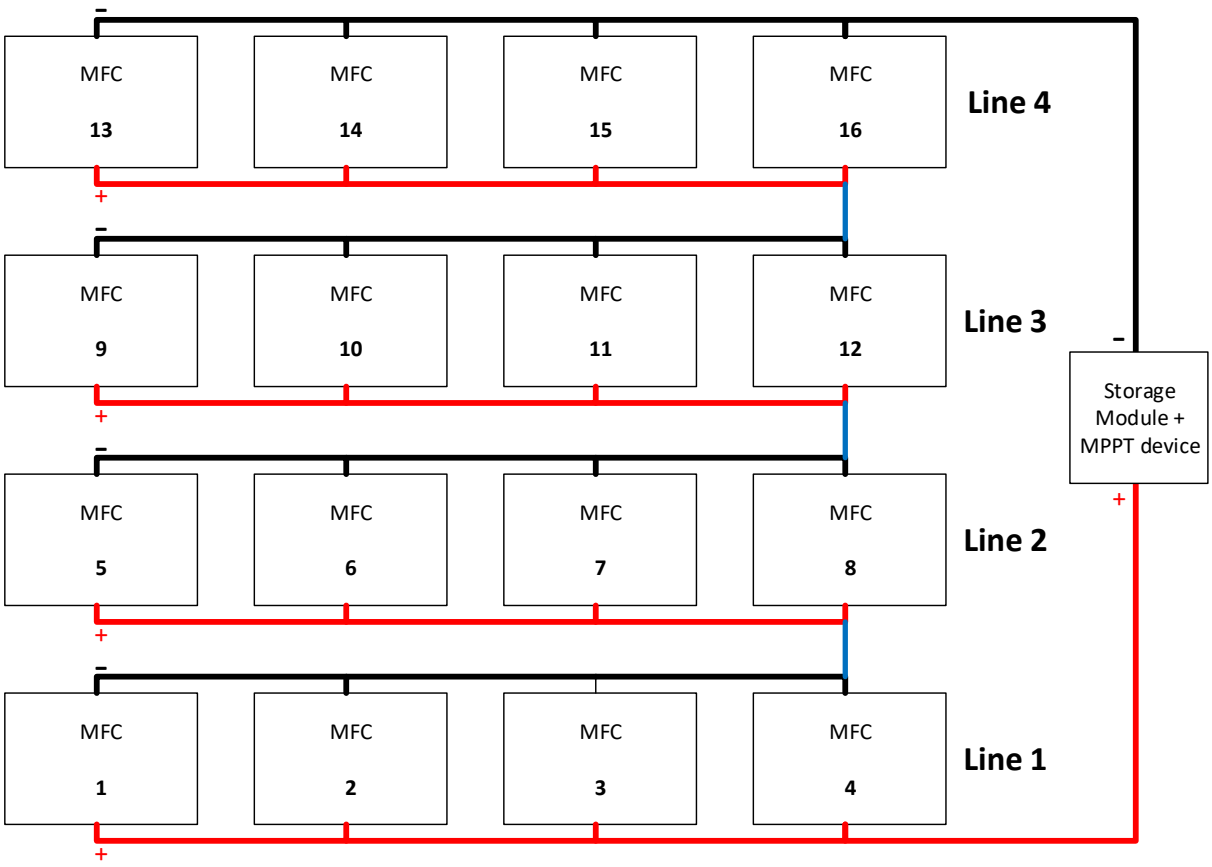

Figure 7: *Representation of the electrical configuration of 16 MFCs and a storage module for one cart of four. Red lines show anodic connections, whereas black lines are for cathodic ones. The blue sectors indicate serial connections.*

The cells included in the same treatment line were connected in parallel implying that the potential of each cell was identical to the potential of the entire line (e.g. $U_{Line\,1} = U_{MFC\,1} = U_{MFC\,2} = U_{MFC\,3} = U_{MFC\,4}$). The current of a line, on the other hand, was equal to the summation of the current of each cell composing that line (e.g. $I_{Line\,1} = I_{MFC\,1} + I_{MFC\,2} + I_{MFC\,3} + I_{MFC\,4}$).

The serial connection between the treatment lines and storage module indicated that the storage current was the same as the one measured for each line ($I_{Storage} = I_{Line\,1} = I_{Line\,2} = I_{Line\,3} = I_{Line\,4}$), whereas the potential was the result of the addition of the potential of each independent line ($U_{Storage} = U_{Line\,1} + U_{Line\,2} + U_{Line\,3} + U_{Line\,4}$).

2.4 Polarisation Procedure

The polarisation and power curves allow determining important electrochemical parameters such as the maximal power that can be generated by the MFC, the current at that particular point and the internal resistance of the bioelectrochemical system. The determination of the polarisation curves were performed in continuous mode. Wastewater from the primary clarifier of *Châteauneuf* WWTP was constantly supplied by a peristaltic pump to the 4 anodic lines of the 1000-L MFC. The flow rate was set to 10 L/h per line. The same flow rate was employed to pump water from the groundwater source and introduced it to the 4 cathodic lines. The air pressure for the bubbling was set to 0.5 bar. A resistance box was employed to vary the external load of the system and a multimeter was linked to follow the cell potential as a function of the applied external resistance. A 100 kΩ resistance was set overnight to reach steady state conditions before polarisation experiments. The external resistance was then modulated from 100 kΩ to 10 Ω and the cell potential monitored. Each resistance was maintained for a period of 15 min. All polarisation curves were realised during period without precipitations.

The resulting potential (U $[V]$) of the electrical circuit as a function of the external resistance (R $[\Omega]$) was directly measured from a multimeter, whereas the external resistance was set with the resistance box. The current (I $[A]$) passing through the resistance was calculated according to Ohm's Law (*Eq.3*). The power (P $[W]$) generated by the system was deduced from the previous equation and defined in the following manner (*Eq.4*).

$$U = RI \qquad (3) \quad and \quad P = UI = \frac{U^2}{R} \qquad (4)$$

In order to obtain values for current and power density, the system was normalised as a function of the anolyte volume (in cubic meter) passing through the system. In continuous mode that volume depended on the anolyte flow rate, in batch mode it was defined as the content of the anodic compartment. The maximal power density generated by the MFC was calculated from the power curve (*Fig.9A*) where the power density was described as a function of the current density of the system. The maximal power density corresponded to the summit of the obtained parabola, which was calculated based on the derivative of the corresponding quadratic equation (*Eq.5*):

$$y = ax^2 + bx + c \qquad (5)$$

Therefore, the maximal power density corresponded to the left coordinate of the following equation (*Eq.6*). At that precise point, the resulting current density was defined as the second coordinate.

$$\left(\frac{4ac - b^2}{4a} ; \frac{-b}{2a} \right) \qquad (6)$$

The internal resistance of the system could be obtained from the polarisation chart (*Fig.9B*) where the potential of the cell was described as a function of the generated current. The internal resistance corresponded to the slope of the polarisation curve (*Eq.7*):

$$R = \frac{\Delta U}{\Delta I} \qquad (7)$$

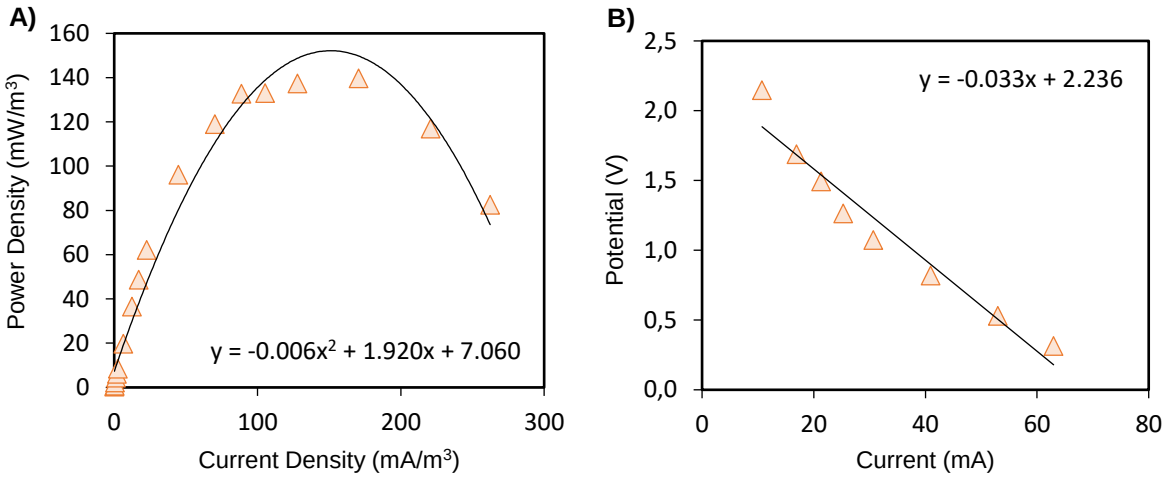

Figure 8: *Examples of a power curve (**A**) and a polarisation curve (**B**).*

2.5 Chemical Oxygen Demand Removal & Coulombic Efficiency

The chemical oxygen demand was determined by using Nanocolor® tube tests (*Fig.10A*). This procedure was based on ISO regulation 15705:2002. Samples were oxidized in a standard manner by chemical digestion using sulphuric acid and potassium dichromate in the presence of silver sulphate and mercury (II) sulphate. Silver acted as catalyst to oxidize the more refractory organic matter. Mercury reduced the interference caused by the presence of chloride ions. The amount of dichromate used in the oxidation of the sample was determined by measuring the absorbance of Cr (III) formed at a wavelength of 600 nm. Absorbance measurements were performed in a digestion tube and converted to COD values, which allowed determining the organic pollutants removal efficiency.

During the procedure, 2 mL of sample was introduced in a testing tube where all reagents were pre-dosed by the kit manufacturer (*MACHEREY-NAGEL GmbH & Co.*). The testing tube was then manually agitated and placed into a heating block (*Fig.10B*) where it was heated at 148°C during 2 h. After a period of 10 min, the testing tube was agitated and cooled to room temperature. The testing tube was then introduced into the spectrophotometer (*Fig.10B*) at 600 nm to determine the Cr (III) absorbance which allowed deducing oxygen consumed during the oxidation and determining the chemical oxygen

demand of the tested sample. The samples that could not be processed immediately after sampling were placed in a freezer of -21°C to avoid any degradation of the organic matter.

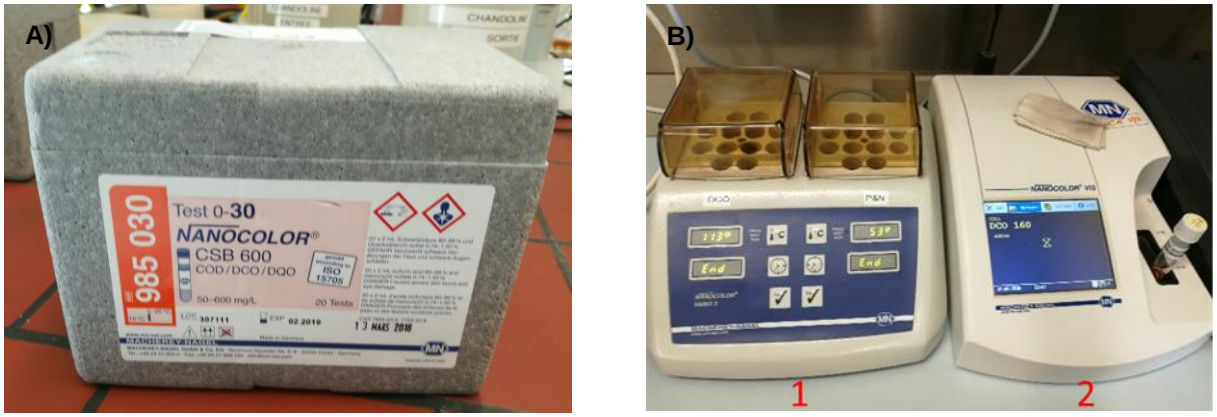

Figure 9: ***A****) Nanocolor® kit employed for COD determination.* ***B****) Heating block (1) and photometer (2) used during the COD measurement procedure.*

The removal effectiveness (ϵ_{COD} [%]) was calculated as the ratio between COD values at the inlet (COD_{in} [$mg\ O_2/L$]) and outlet (COD_{out} [$mg\ O_2/L$]) of the 1000-L MFC (*Eq.8*):

$$\epsilon_{COD} = \frac{COD_{in} - COD_{out}}{COD_{in}} \cdot 100 \qquad (8)$$

The Coulombic efficiency (CE) is the ratio of the total electrical charge (Coulomb) transferred to the anode from the substrate to the maximum possible transferable charge if all organic matter produced current [22]. In other terms, it indicates the proportion of degradable matter that was converted into electrical current. The fraction that was not transformed into electricity was either related to biomass formation or used in competitive reactions with alternative electron acceptors [23] present within the MFC anolyte. The Coulombic efficiency (ϵ_{Cb}[%]) was evaluated differently depending working in batch (*Eq.9*) or continuous mode (*Eq.10*):

$$\epsilon_{Cb} = \frac{M \int_0^t I\, dt}{F\ b\ v_{An} \Delta COD} \cdot 100 \qquad (9) \quad or \quad \epsilon_{Cb} = \frac{M\ I}{F\ b\ q_{An}\ \Delta COD} \cdot 100 \qquad (10)$$

$M = 32$ [g/mol]: the molecular weight of O_2, $F = 96485$ [C/mol]: Faraday's constant, $b = 4$ [$-$]: the number of electrons exchange per mole of oxygen, I [A]: the current generated by the MFC, ΔCOD [$mg\ O_2/L$]: the COD change over time (*Eq.9*) or the difference in the influent and effluent COD (*Eq.10*), t [s]: the process duration, v_{An} [m^3]: the anolyte volume and q_{An} [m^3/s]: the anolyte flow rate.

2.6 Normalised Energy Recovery

The Coulombic efficiency is an important indicator concerning the performance of MFCs but should not be presented alone because it is based on current measurements only. However, the maximal power output of the system does not always occur at the highest current generation and, therefore, important CE values do usually not mean high-energy production [24], especially when using MPPT devices favouring power output instead of current production. An alternative indicator is the normalised energy recovery (NER), which quantifies the amount of energy generated by the installation and provide a point of comparison between the different MFC technologies developed. The energy recovery can be normalized as a function of the volume of treated wastewater (NER_V $[kWh/m^3]$, *Eq.11*) or the quantity of COD removed (NER_{COD} $[kWh/kg\ COD]$, *Eq.12*).

$$NER_V = \frac{\int_0^t P\ dt}{v_{An}} = \frac{\bar{P}}{q_{An}} \qquad (11) \quad and \quad NER_{COD} = \frac{NER_V}{\Delta COD} \qquad (12)$$

P $[kW]$: The power generated by the 1000-L MFC ($\bar{P}$ refers to the average power), t $[h]$: the process duration, v_{An} $[m^3]$: the anolyte volume, q_{An} $[m^3/h]$: the anolyte flow rate and ΔCOD $[g\ O_2/\mathrm{m}^3]$: the COD change over time or the difference between influent and effluent COD.

By comparing the experimental energy generated per kilogram of COD to 3.86 kWh (the maximal energy theoretically recoverable from the complete oxidation of 1 kg of COD to CO_2 and H_2O [25,26]). It is possible to assess the energy efficiency (EE) (ϵ_{En} [%]) of the system (*Eq.13*), which can be used as a complementary indicator to the Coulombic efficiency.

$$\epsilon_{En} = \frac{NER_{COD}}{3.86\ kWh/kg\ COD} \cdot 100 \qquad (13)$$

2.7 Soluble O_2 Efficiency Determination

The determination of the concentration of soluble O_2 was performed using a dissolve oxygen probe (HI2040 edge, *Hanna instruments*). The tested samples were collected in 50 mL-falcon tubes, which were completely sealed to ambient air, and the measurements performed swiftly upon sampling in order to avoid any possible external influence. A volume of 40 mL was delicately poured into a 100 mL glass beaker, placed on a magnetic stirrer. The probe was submerged into the stirred solution (150 rpm) until stabilisation (~ 1 min) and the value recorded. The dissolved oxygen within both anolyte and catholyte plays a major role in the optimisation of the energy generated by the 1000-L MFC because oxygen is an important electron acceptor and the electrons generated during the oxidation of the organic matter

will tend to be transferred to O_2 to reduce it into water (*Eq.1*). If dissolved oxygen is present in the anolyte in high concentration, the electrons generated during the process will react with it instead of passing through the external electrical circuit to produce electricity. In that case, the system efficiency will be reduced. In order to boost the energy output, the difference between the dissolved O_2 of the catholyte and anolyte has to be maximized. The highest difference would be when dissolved oxygen reaches maximal solubility in the catholyte and when the anolyte is completely depleted of oxygen. The next formula (*Eq.14*) was established to gauge the relative efficiency of the system regarding oxygen (ϵ_{O_2} [%]):

$$\epsilon_{O_2} = \frac{O_{2\ catholyte} - O_{2\ anolyte}}{O_{2\ catholyte\ (\max)}} \cdot 100 \qquad (14)$$

2.8 ICP-OES Analytical Technics

The inductive coupled plasma optical emission spectrometry (*Varian 720-ES ICP Optical Emission Spectrometer*) is a kind of elemental analysis that allows the determination of the presence of metals within aqueous samples, along with the quantification of the detected metals. This technique is based on spontaneous emission of photons from atoms and ions that have been excited [27].

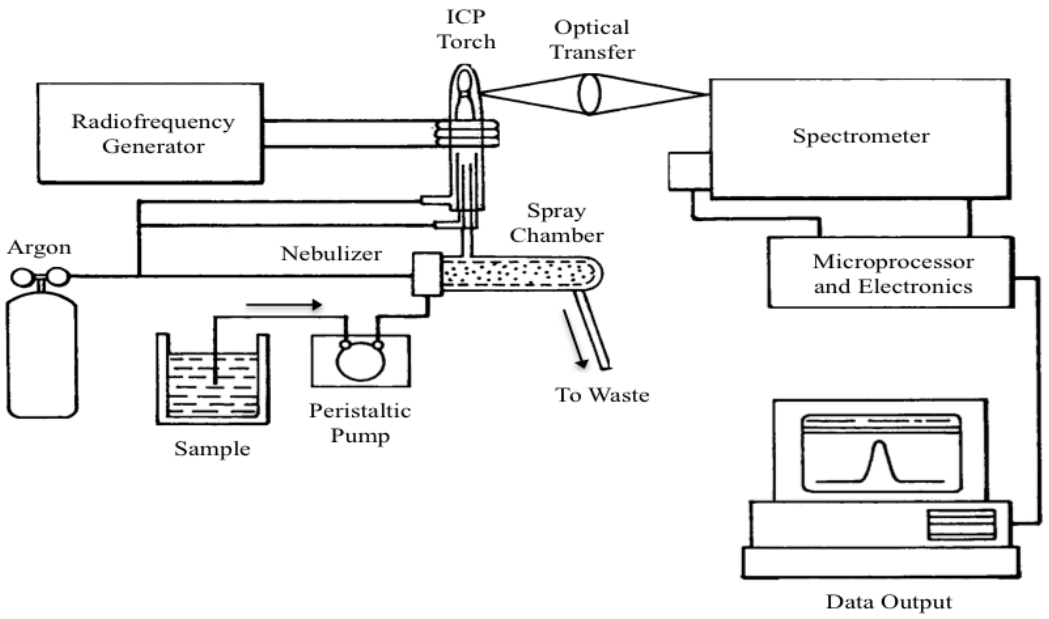

Figure 10: *Scheme of the ICP-OES working principle, adapted from literature [28].*

The working principle is quite simple (*Fig.11*). Liquid samples are converted into an aerosol by a nebulizer *(Agilent Technologies*) and directly injected into a radiofrequency induced argon plasma. At that location, samples are quickly vaporized due to the high temperature of the plasma, up to 10'000 K at the plasma core (*Quartz Torch Agilent ICP-OES Axial*). The elements present within the samples are,

therefore, liberated as free atoms. The collisions of these new liberated atoms impart additional energy to themselves. They are, therefore, converted into ions that are promoted to certain excited states. The ionic particles then relax to the ground state by emitting a photon of characteristic wavelength. The total number of photons is directly proportional to the concentration of the originating element of the sample and can be determined by analysing the wavelength. When the wavelength exits the monochromator, it is converted to an electrical signal that is amplified and displayed on a computer.

The data were depicted as absorbance pics. In order to determine the concentration from the obtained signals, a calibration curve was established by preparing several different standards from specific atomic absorption spectroscopy solutions (AAS) in accordance with the ions of interest. The standards were made by dilution with aqueous HNO_3 2%, which served as matrix for the analysis. The calibration curve permitted calculating the concentration of the chosen ion from the intensity of the recorded signal. It was important for the acquisition of accurate data that the concentration of the measured element was within the range of calibration. Samples were, therefore diluted with the same analytical matrix.

2.9 Metagenomics 16S rRNA V4-V5 Analysis

In order to determine the microorganisms involved in the microbial fuel cell installation, the biofilms present on the electrodes were sampled (*Fig.12*) with a sterile homemade sampling tool (ID = 8 mm), directly on the RVC anodes on the side facing VANADion™ membranes. Two pieces of RVC with a projected surface of 0.5 cm^2 each were taken to ensure to optain bacteria on the electrode's surface.

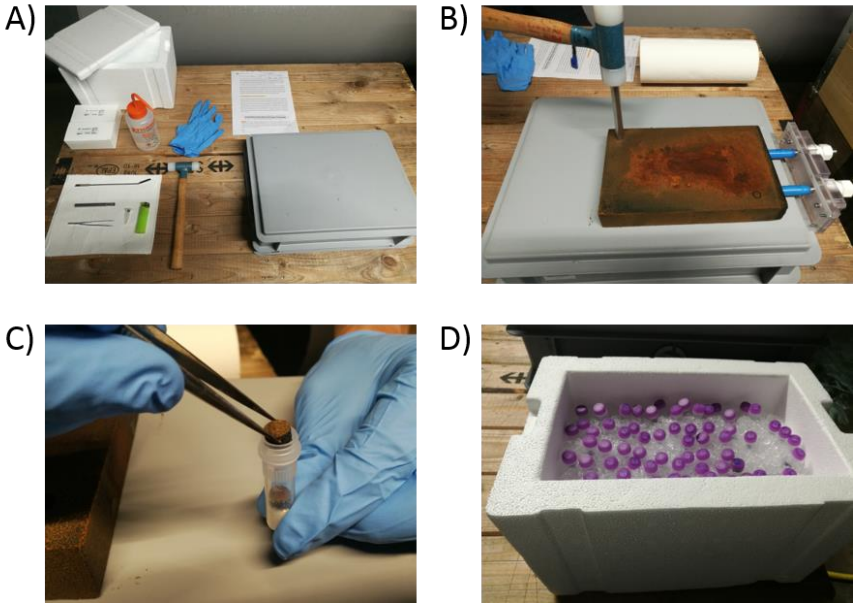

Figure 11: *Sampling material (**A**) to collect small fractions (0.5 cm^2) of RVC electrode with biofilm at the interface. The sterilisation process was performed by a flame using ethanol as fuel. The samples were taken at the top-right and bottom-left part of each electrode (**B**) and introduced into tubes containing a lysing matrix (**C**). They were then transported on ice (**D**) and stored at -21.0°C until DNA extraction.*

A total of 64 samples were collected, one for each first anodic electrode of every single microbial fuel cell reactor unit. The sample identification was realized in accordance with the scheme below (*Fig.13*).

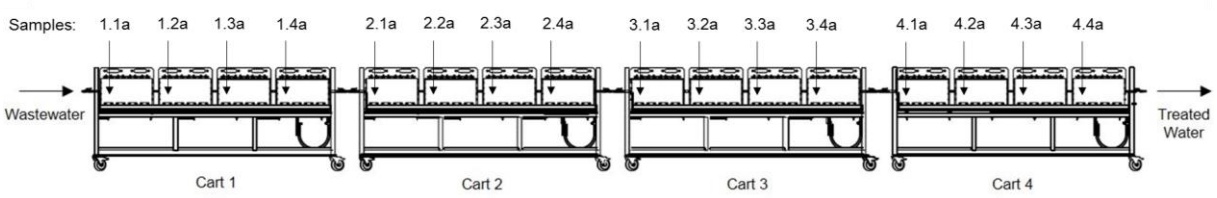

Figure 12: *Frontal view (anodic compartments) of the microbial fuel cell stacks with the first treatment line on direct display: 16 MFC units divided onto 4 carts. The sampling locations for metagenomics analysis were noted from 1.1a to 4.4a. The same notation was adopted for the other treatment lines for the stacks behind the first visible line of MFC units, except the alphabetical letter that changed as a function of the position of the stack: line 2 = b, 3 = c and 4 = d.*

The DNA extraction was realized according to the protocol provided by the manufacturer of the FastDNATM SPIN Kit for Soil (*MP Biomedicals*). Point 4 of the protocol was modified. A Precellys 24 homogenizer (*Bertin instruments*) was used instead of a FastPrep instrument. DNA quantification was realized with a QubitTM dsDNA HS Assay Kit (*Invitrogen*) to be sure that the concentration of DNA was high enough for sequencing (> 1 ng/µl).

DNA extracts were sent to the IMR centre for comparative genomics and evolutionary bioinformatics (*Dalhousie University, Canada*). DNA samples were sequenced using 16S rRNA Bacteria V4-V5 amplicons.

2.10 NH_4^+ / NO_3^- Analysis & Denitrification Calculation

Ammonium concentration was determined by the indophenol method [29], where ammonium reacts with hypochlorite and salicylate in the presence of sodium nitroprusside as catalyst to form blue indophenol, which is easily quantified via UV/Vis spectrophotometry at 690 nm. During the analysis, 0.2 mL of sample was introduced to a testing tube where all reagents were pre-dosed by the kit manufacturer (*MACHEREY-NAGEL GmbH & Co.*). The testing tube was then manually agitated. After a reaction time of 15 min (20-25°C), the testing tube was placed in the spectrophotometer for direct measurement.

Nitrate concentration was determined by the 2,6-dimethylphenol spectrometric method [30], where in acidic solution nitrate ions reacted with 2,6-dimethylphenol to form 4-nitro-2,6-dimethylphenol, which can be evaluated photometrically at 350 / 365 nm. During the analysis, 0.5 mL of sample was introduced within a testing tube where all reagents were pre-dosed by the kit manufacturer (*MACHEREY-NAGEL GmbH & Co.*). The testing tube was then manually agitated. After a reactional period of 10 min (20-25°C), the testing tube was placed in the spectrophotometer for direct measurement.

For both analysis, the samples that could not be processed immediately after sampling were placed in a freezer at -21.0°C to avoid any degradation.

2.11 Theoretical Oxygen and Air Consumption

The theoretical oxygen consumption rate ($\dot{O}_{2_{Cons}}$ $[kg/day]$, *Eq.16*) for biological treatment in MFC depends on the concentration of organic matter removed during the purification process (ΔCOD $[g\ O_2/m^3]$, *Eq.15*) as well as the flow rate of wastewater treated (q_{An} $[m^3/day]$). A more polluted water will required a larger amount of oxygen. The same applied when a bigger volume of wastewater was considered. This O_2 consumption rate can be converted to the minimal air supply ($\dot{Air}_{Cons}$ $[m^3/day]$, *Eq.17*) needed for wastewater treatment. In this equation (*Eq.17*), $\rho_{O_2} = 1.429$ $[kg/m^3]$ is the density of oxygen under standard conditions and $V_{O_2} = 20.95$ $[\%]$: the proportion (v/v%) of oxygen present in air.

$$\Delta COD = COD_{in} - COD_{out} \quad (15)$$

$$\dot{O}_{2_{Cons}} = \Delta COD \cdot q_{An} \quad (16)$$

$$\dot{Air}_{Cons} = \frac{\dot{O}_{2_{Cons}}}{\rho_{O_2} \cdot V_{O_2}} \quad (17)$$

The actual air consumption is much higher due to limited oxygen mass transfer through the air-water interface.

2.12 Smartphone Recharge

Smartphone recharging was performed with the components displayed in the next picture (*Fig.14*). A fully charged 3.7 V lithium battery (Li - Mn 3.7 V / 2250 mAh, *Sony*) was directly plugged with a power bank (Bolt alu power bank 2200 mAh, *Bullet*) that allowed to transfer the energy stored in the battery (by 16 cells of the MFC installation) to the smartphone (Honor 8 FRD-L09, *Huawei*). A wattmeter (Multifunction USB tester, *Atorch*) was connected in-between to monitor the electrical charge (q $[mAh]$) and energy (E $[Wh]$) transferred as well as the recharge time (t $[min]$) and setup temperature (T $[°C]$). The smartphone recharging was monitored thought its battery status display (S $[\%]$).

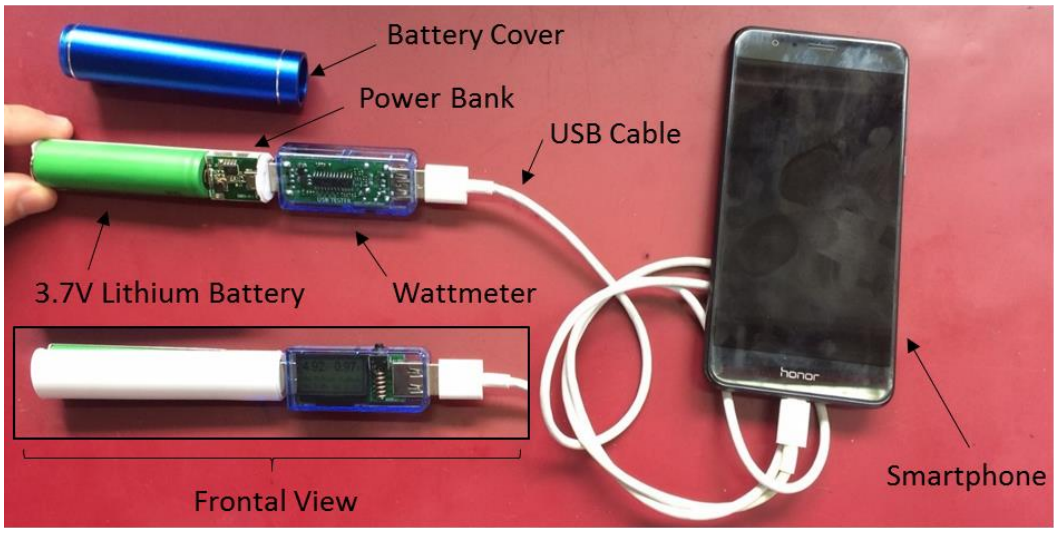

Figure 13: *Devices for smartphone recharge. A fully-charged 3.7 V lithium battery was introduced into a power bank with a wattmeter connected to a USB port. The second USB port of the wattmeter was linked to a smartphone with a USB cable.*

The batteries specifications are displayed in the following table (*Tab.1*):

Battery Type	Rechargeable	Smartphone
Model	US18650V3	HB366481ECW
Technology	Lithium-ion	Lithium-ion
Capacity (Charge)	2150 mAh	2900 mAh
Capacity (Energy)	7.69 Wh	11.46 Wh
Voltage	3.70 V (up to 4.2 V)[1]	3.82 V (up to 4.4 V)

Table 1: *Specifications of the batteries employed to store the energy produced by a 250 L section of the MFC installation and the battery included in the smartphone. Note 1: the maximal charge voltage of the batteries have been set to 4.1 V in order to preserve the energy storing modules. This represents a capacity difference of approximatively 12.5%, which resulted in a maximal storage energy of 6.73 Wh instead of 7.69 Wh.*

2.13 Gas Analysis

Gases were sampled with a Luer Lock syringe (*BD Plastipak*). A volume of 30 mL was withdrawn from the first/second anodic headspace (capacity: 1.95 L) of each treatment line (*Fig.13, 1.1 & 1.2a-d*). The samples were injected in a micro-GC 490 (*Agilent*) mounted with two columns (MS5A and PPU). The MS5A column was used to analyse H_2, O_2, N_2 and CH_4, while the PPU was employed to quantify CO_2 and CH_4. The first column was heated at 90°C and operated at a pressure of 150 kPa. The same pressure was set for the PPU column, but at a temperature of 80°C.

3 Results and Discussion

3.1 Process Optimisation

Several parameters could impact on the wastewater treatment process when operating the 1000-L MFC. These parameters included oxygen and wastewater flow rates as well as different electrical loads (either fixed external resistances employed for polarisation purposes or modulable resistances used for charging batteries) applied to each MFC-sub-stack.

3.1.1 O_2 and N-Species Effect on MFC performance

In order to understand the impact of oxygen and possible nitrogen species on the performance of the 1000-L MFC, a batch (catholyte) experiment was performed where the power output of the system was monitored over time. During this procedure, the O_2 catholyte supplied was interrupted between on day 8 to 10 and oxygen concentration dropped from 7.85 to 0.07 mg/L. In this period, the average power output decreased from 0.165 to 0.029 W (*Fig.15*), meaning that O_2 contributed by 82% (0.136 W) to the electron flux from anode to cathode. The other part of the electrons transferred (18%) were mostly used to reduced N-species into N_2 gas, participating to the water denitrification process, or employed by alternative electrons' acceptor species potentially present in groundwater.

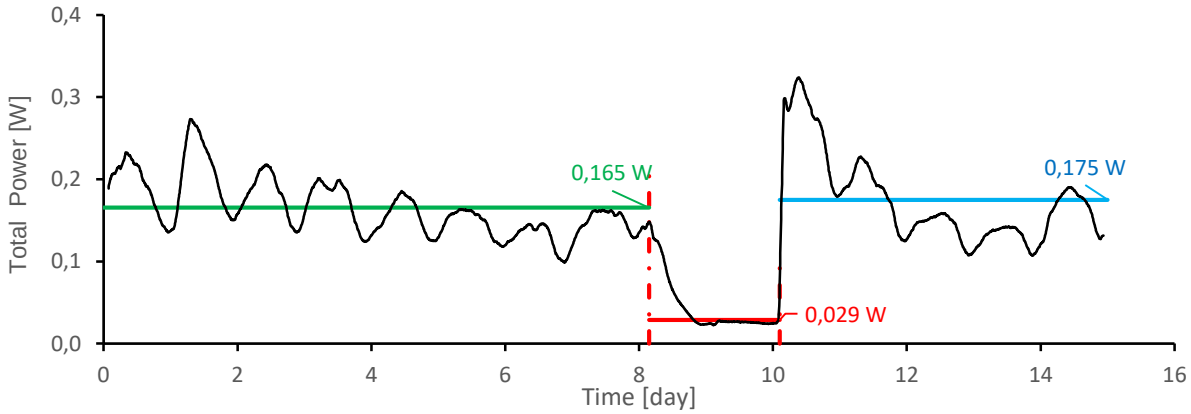

Figure 14: *Power generated by the 1000-L MFC over time. The anodic compartment was feed (20 L/h) with wastewater, whereas oxygenated (0.5 bar air bubbling in batch mod) groundwater was used as catholyte. The air supply was stopped between day 8 and 10. The energy produced under MPPT and stored on lithium batteries.*

The used of oxygen as electron acceptors in the 1000 L-MFC system was a necessity for two main reasons. O_2 permitted boosting the overall performance of the 1000-L MFC by a factor 6.0 and it could also affect the denitrification process in a positive manner by increasing the part of NH_4^+ removed [31].

3.1.2 Oxygen Flow Rate Regulation

There were three different useful criteria for assessing the impact of oxygen concentrations on the performance of the 1000-L MFC. The energy produced by the system (*Sec. 3.2*) was one of them in addition to the defined O_2 efficiency (*Sec. 3.7*) as well as the chemical oxygen demand (*Sec. 3.5*).

To investigate the impact of oxygen on the system, the air pressure employed for air bubbling in the cathodic compartments was reduced from 1.0 bar to no pressure at all. All experiments were performed, for a period of 64 h, in an anolyte batch configuration. The catholyte was introduced in a continuous manner at a constant flow rate of 3.35 L/h per line. The potential of each cart was monitored with the help of a multimeter connected to a decade box, configured with a resistance of 1000 Ω. One day prior to the experiment, the system was flushed with new anolyte and catholyte with a total flow rate of 40 L/h in both compartments. This step was performed to ensure that fresh media was present when starting the experiment.

The energy output generated by the 1000-L MFC varied as a function of the air pressure employed to increase the oxygen concentration in the catholyte. Next chart (*Fig.16*) illustrates this variation.

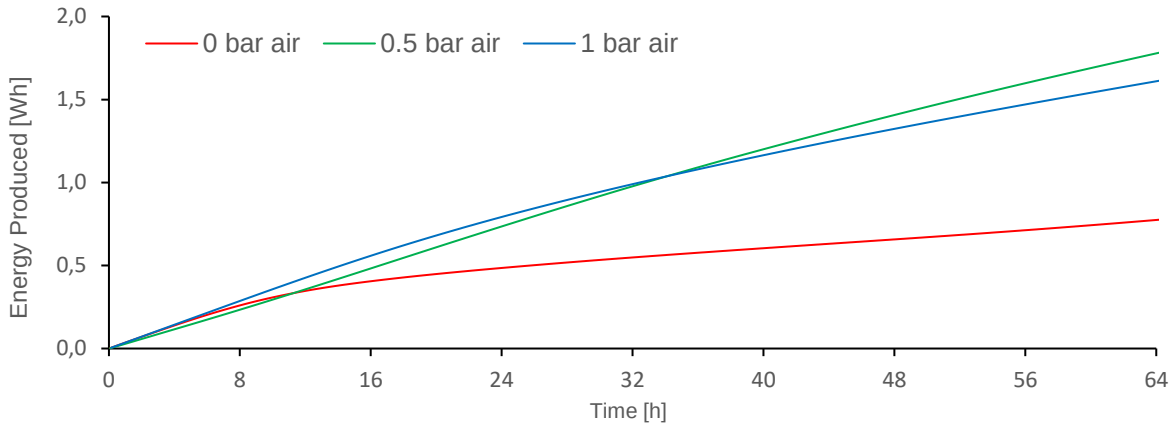

Figure 15: Total *energy profile using different air bubbling conditions (0, 0.5 and 1.0 bar). The anolyte was wastewater from the primary clarifier of Châteauneuf WWTP and not recirculated. The catholyte (groundwater) was constantly feed to the system at a flow rate of 13.3 L/h.*

It was clear that without air bubbling, less energy was generated (only 0.77 Wh for 64 h) due to the fact that the groundwater contained only a limited amount of oxygen (< 0.1 mg O_2 /L). Therefore, the electron transfer from anodic to cathodic compartment was limited. When oxygen was supplied to the system, through air bubbling, the energy output obtained after a period of 64 h increased to 1.61 Wh (1.0 bar) and even reached 1.78 Wh when 0.5 bar was applied. These results demonstrated the need to supply additional air-oxygen for electricity generation and purification. The process was 2.3 times more efficient when working with an O_2 supply of 0.5 bar (*Sec. 4.1.1*).

In the following table (*Tab.2*), the dissolved oxygen concentration of both anolyte and catholyte after 64 h of process are displayed as well as their corresponding oxygen efficiency.

Conditions	*Dissolved O_2 Anolyte (mg/L)*	*Dissolved O_2 Catholyte (mg/L)*	*Oxygen Efficiency (%)*
0.0 bar	0.01	0.07	0.70
0.5 bar	1.88	8.18	73.7
1.0 bar	6.67	8.44	20.7

Table 2: *Dissolved oxygen present in anolyte and catholyte as well as defined oxygen efficiency for the three air bubbling pressures (0, 0.5 and 1.0 bar).*

The first observation concerned the oxygen efficiency. In order to work under optimal conditions, a air bubbling pressure of 0.5 bar should be chosen. Indeed, at that pressure the oxygen efficiency was much higher than in the other two experiments with zero and 1.0 bar. When using an air pressure of 1 bar, the dissolved oxygen concentration of the catholyte increased from 8.18 to 8.44 mg/L, which was advantageous for energy production. However, the major drawback when using higher air pressure (1.0 bar) to supply oxygen in the catholyte was that an important concentration of O_2 superior to 6.6 mg/L was found in the anolyte as well. Such a high concentration could be explained by the oxygen saturation of the catholyte and strong bubbling that favoured O_2 transfer through the membrane into the anodic compartment. Strong air bubbling should therefore be avoided as it does not increasing the power output of the MFC. When no air was supplied to the MFC cathodes, the catholyte contained less oxygen (0.07 mg O_2/L) and resulting in a lower oxygen efficiency.

The chemical oxygen demand for the three air-oxygen bubbling conditions was investigated to see if any notable difference was observable. The difficulty of the comparison was the distinct initial values of COD for wastewater, ranging from 82 to 231 mg/L, due to the changing composition of the effluents entering the WWTP. However, the purified wastewater was leaving the installation with COD values between 46 and 51 mg/L. From this subjective comparison, it appeared that the best removal efficiency was obtained at 0.5 bar with an efficiency close to 80% (*Tab.3*). The efficiency was less important under the 2 other conditions, which suggested that an enriched O_2 catholyte could increase the removal capability of the system.

Conditions	*Initial COD (mg/L)*	*Final COD (mg/L)*	*Removal Efficiency (%)*
0.0 bar	82.5	46.7	43.4
0.5 bar	231	48.3	79.1
1.0 bar	135	50.2	62.8

Table 3: *Initial and final chemical oxygen demand values for wastewater as well as removal efficiency for the three different air bubbling conditions (0, 0.5 and 1.0 bar). The COD values were adapted for a wastewater purification period of 64 h, under batch condition.*

3.1.3 MPPT Device and its Implementation

Another way to increase the current generated by the MFC-Sub-Stacks was to vary the external loads using resistances decade boxes or maximal power point tracking devices. The decade boxes allowed manually changing the external resistance, whereas MPPT systems automatically adapted the resistance to maximise the power output of the Sub-Stacks. Following Ohm's law (*Eq.3*), a lower external load increased the quantity of current passing through the electrical wires (*Fig.17*), hence higher Coulombic efficiencies. A direct correlation between the current generated by the MFCs and its associated Coulombic efficiency was experimentally observed as expected from the CE definition (*Eqs. 9/10*). The MPPT devices were considered to be assets for the MFC installation because they improved the MFCs efficiency in terms of energy output as well as current generation. They were implemented into each MFC-Sub-Stack for further experimentations, and were especially helpful regarding flow rate investigations. Next chart (*Fig.17*) demonstrates the impact of the external resistance on currents generated and Coulombic efficiencies.

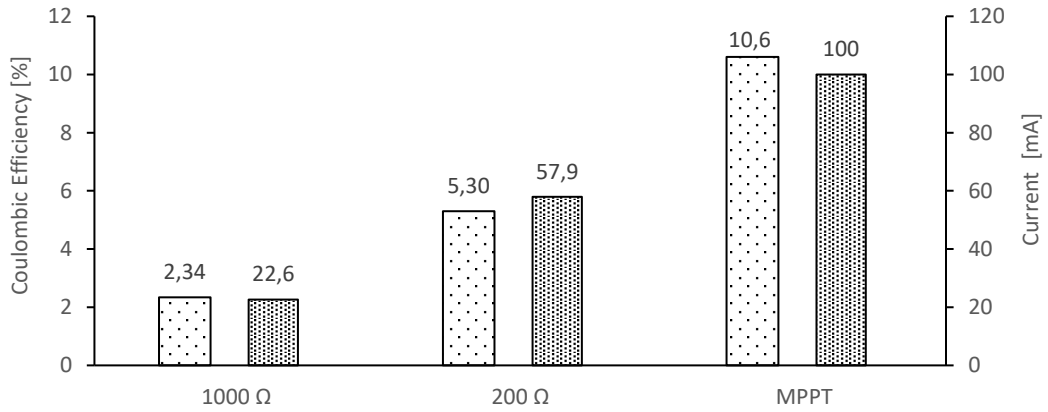

Figure 16 *Impact of different external resistances on CE (sparse dots) and current production (compact dots) under the following conditions: $q_{an} = q_{cat} = 6.7$ L/h and $P_{air} = 0.5$ bar. The MPPT devices allowed optimising power output of the system by adapting the external resistance. Resistances < 35 Ω were determined as optimal values. The total projected anodic surface available was 7.0 m^2 giving normalised currents of 3.23, 8.27 and 14.3 mA/m^2 for fixed resistances of 1000 and 200 Ω as well as MPPT systems.*

3.1.4 Anolyte Flow Rate Variation

Parameters such as anolyte and catholyte flow rates were also varied to understand their impact on the performance of the 1000-L MFC. The Coulombic efficiency was affected by the flow rate of wastewater passing through the MFC units for purification. Higher CEs were obtained at lower flow rates (*Fig.18*), what was in line with previous studies [32, 33]. The average Coulombic efficiency reached 14.9% for a wastewater flow of 1.3 L/h, whereas a peak efficiency of 25.2% was obtained considering maximal currents (average on the top 2.5% recorded values). However, the Coulombic efficiency is not always the best indicator for MFCs effectiveness because it accounts only for current generation. With the use

of the batteries charging modules, which were manufactured with maximal power point tracking devices (*Sec. 3.2; Fig.7B*), power generation (up to 0.65 W) was favoured at the expense of current produced. The Coulombic efficiency values were underestimated. The energy efficiency was employed as an alternative indicator to assess the 1000-L MFC in terms of energy generation. The energy efficiency was calculated by comparing the energy density obtained experimentally (0.47, 0.33 and 0.22 kWh/kg COD for 1.3, 6.7 and 40 L/h, respectively) to the theoretical value of 3.86 kWh (energy generated for the complete oxidation of 1 kg of COD). This indicator increased with lower flow rates (*Fig.18*). However, energy generation using MFC might be limited by various factors that could reduce the MFCs power generation output. Possible sinks of electrons included [34]: oxygen reduction, methanogenesis, H_2 production by fermentation, oxidation by electron acceptors present in the anolyte [23], bacterial growth, Fe^{3+} and other metal reduction as well as sludge sedimentation. Coulombic and energy efficiencies will increase by preventing these side reactions. To realize this: particulate sludge needs to be removed possible with a better MFC unit design, automatized oxygen dosage should help to further reduce oxygen migration into the cathode, and in general a better mass balance will eliminate errors in the assessment as the hypothesis is that the present performance is underestimated.

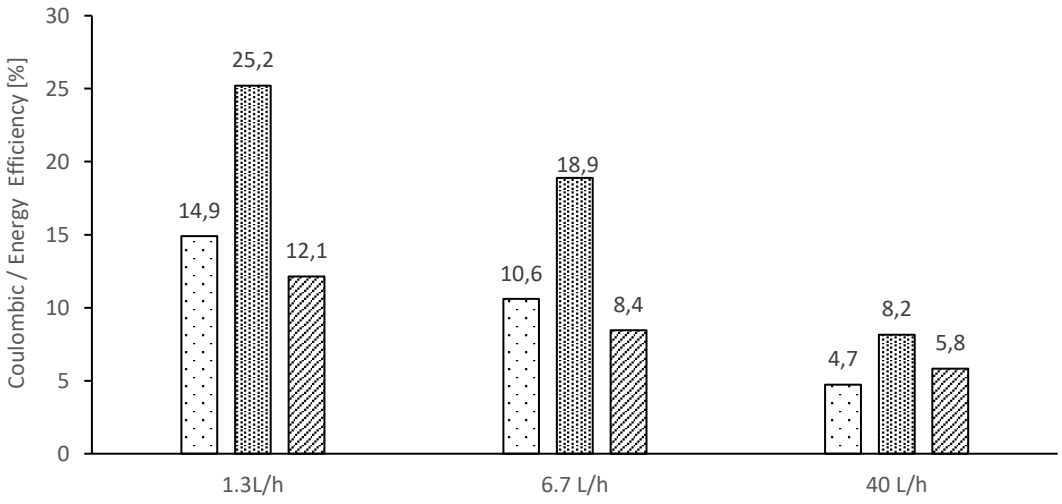

Figure 17: *Comparison of wastewater flow rates and their impact on average and maximal CE (sparse and compact dots) as well as on Energy Efficiency EE (dashed line) under the following conditions:* q_{cat} *= 6.7 L/h,* P_{air} *= 0.5 bar and MPPT.*

Even though the lowest flow rate permitted reaching the best efficiency, it was the opposite when looking into absolute energy production values. Only an energy of 1.24 Wh could be generated with an anolyte rate of 1.3 L/h, whereas 13.0 Wh was obtained for 40 L/h (2.30 Wh for 6.7 L/h). Therefore, at higher flow rates the system lost in Coulombic and cleaning efficiency but more energy was recovered and a higher volume of wastewater treated but with reduced organic matter degradation (*Sec. 4.2.3*).

The next primordial question was how it will affect the purification level of wastewater.

3.2 Wastewater Purification Level

3.2.1 Swiss Legislation Requirement (COD)

Most countries regulate wastewater disposal. A certain effluent quality has to be achieved before its release into the environment. The Swiss legislation fixed the limits regarding organic pollutant removal (chemical oxygen demand) by the Water Protection Ordinance (WPO, 2018) [35]. The limit depends on the size of the wastewater treatment plant in terms of population equivalent (PE), which is a conventional unit, used to measure the daily pollution generated per inhabitant. The pollution produced by an industry is also converted into population equivalents by using the relations defined in the subsequent table (*Tab.4*) [36]:

1 PE hydraulic	=	170	L / day
1 PE DBO_5	=	60	g O_2 / day
1 PE COD	=	120	g O_2 / day
1 PE N-NH_4	=	6.5	g N-NH_4 / day
1 PE P_{tot}	=	1.8	g P / day

Table 4: *Conversion units to transform daily loads into population equivalents (PE).*

For instance a cheese factory that generates a daily organic load of 1080 g DBO_5 per ton of transformed milk with a hydraulic load of 2000 L corresponds to a biochemical PE of 18.0 with a hydraulic PE of 17.8. Therefore, the factory generates as much pollution as 18 inhabitants. WWTPs can determine their actual treating capacity in terms of population equivalents by measuring the volume and organic load of wastewater at their inlet.

Regarding the COD legislation, two different cases are distinguished and summarized in the following table (*Tab.5*):

WWTP Conditions / Limitations	*< 10'000 PE*	*> 10'000 PE*
Discharge Concentration (mg O_2/L)	< 60	< 45
Removal Efficiency (%)	> 80	> 85

Table 5: *COD requirements for remaining pollutants in discharged wastewater as required by the Swiss legislation.*

These regulations apply for communal wastewater, including waste from households and similar wastewater as well as precipitation water coming along with domestic water, for an excess of 200-population equivalent.

Châteauneuf WWTP was dimensioned for a total treating capacity of 66'600 PE (8000 kg COD/day). However, the average treating capacity for 2018 was 5650 kg COD/day, which corresponded to population equivalent of 47'000 people. Therefore, the stricter norm applied (< 45 mg/L and > 85%).

3.2.2 COD Kinetics under Batch Conditions

A kinetic study was realized to assess water purification effectiveness of the 1000-L MFC Stack under batch conditions. This kinetic experiment was performed during a period of 65 h. An air pressure of 0.5 bar was applied for groundwater oxygenation as it was found to be the most efficient injecting air pressure (*Sec. 4.1.2*). Prior to the experiment, both anolyte and catholyte were supplied to the reactor with a flow rate of 40 L/h in order to ensure the presence of fresh liquids (wastewater and water) at the beginning of the experimental procedure. Then the anolyte was stopped to establish batch conditions, whereas the catholyte was still supplied to the installation at a reduced flow rate (13.3 L/h). Samples were taken throughout the experiment and the chemical oxygen demand (*Sec. 3.5*) assessed for each of them. In parallel, a 10 L sealed-container was filled with the same wastewater and employed as comparative reference for COD removal.

The MFC scale-up installation permitted purifying wastewater to an efficiency superior to 80%. Indeed the initial chemical oxygen demand decreased from 231 to 44.7 mg/L within 65 h (*Fig.19*). The control, on the other hand, resulted in a removal efficiency close to 22% with an important COD discharge concentration value superior to 180 mg/L. The developed system allowed, thus, boosting the purification level of wastewater by a factor 4.

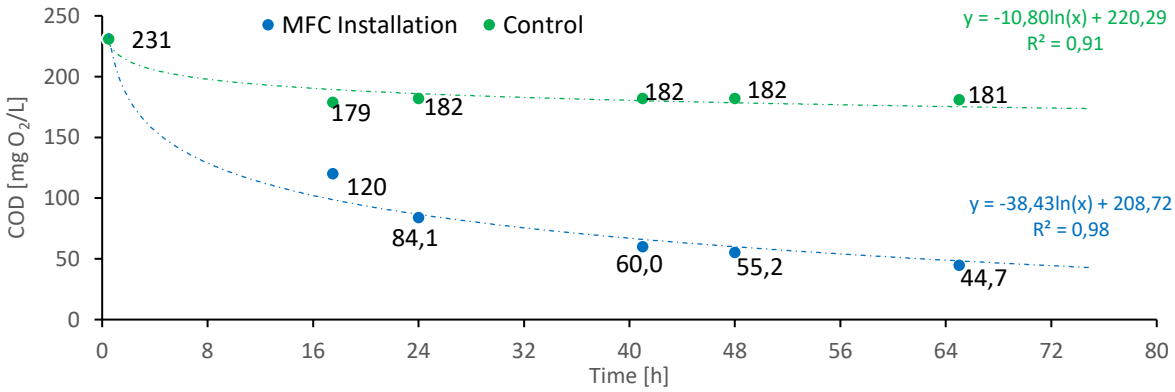

Figure 18: *COD removal kinetics comparison between the 1000-L MFC and a control. The scale-up MFC was working in batch mode regarding the anodic compartment and in continuous manner for the catholyte (13.3 L/h). Air with a pressure of 0.5 bar was bubbling into the cathodic chamber. The control was a 10 L sealed-container filled with the same wastewater as employed in the 64 microbial fuel cells.*

According to the Swiss legislation (*Sec. 4.2.1*), the chemical oxygen demand should be inferior to 60 mg/L (case 1) for WWTP built for less than 10'000 population equivalent (PE) and inferior to 45 mg/L (case 2) for installation treating more than 10'000 PE. These criteria were fulfilled after 40 h for the first case (< 60 mg/L) and 65 h for the second one (< 45 mg/L). Another standard regarding the removal efficiency has also to be respected. An efficiency superior to 80% need to be reached for WWTP < 10'000 PE (case 1) and superior to 85% for WWTP > 10'000 PE (case 2). Within 65 h, the purification

process allowed reaching the norm for small wastewater treatment plant (case 1). By extrapolating these data, the 85% removal mark should be reached after 92 hours (*Fig.20*).

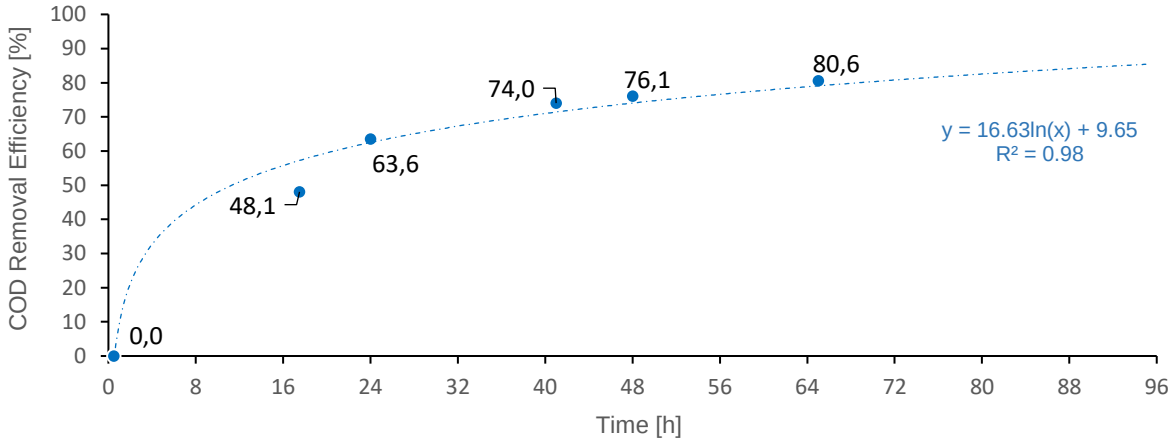

Figure 19: *COD removal efficiency for the 1000-L MFC. The scale-up system was working in batch mode regarding the anodic compartment and in continuous manner for the catholyte (13.3 L/h). Air with a pressure of 0.5 bar was bubbling into the cathodic chamber.*

These results permitted estimating a residence time for the installation, which could be employed to deduce flow rates when working in a continuous manner. Knowing the volume of wastewater employed for each process line (115 L) allowed calculating the flow rate per line needed for wastewater purification (*Tab.6*). A maximal flow rate of 1.70 L/h could be used in the first case, whereas 1.25 L/h in the second one.

Conditions:	*Residence Time (h)*	*Flow Rate (L/h)*	*Daily Volume (L/d)*
COD < 60 mg/L	48	2.40	230
Efficiency > 80%	68	1.70	160
COD < 45 mg/L	72	1.60	150
Efficiency > 85%	92	1.25	120

Table 6: *Estimation of the residence time, flow rate (per treating line) and daily volume that could be purified while respecting wastewater disposal in terms of COD removal. The two limiting cases were separated here.*

These batch experiments constituted a starting point for the implementation of continuous flow in the 1000-L MFC. An anolyte flow rate of 1.3 L/h (*Tab.6*) was first tested in that regard. Afterwards, as the purification met the Swiss regulations, higher flow rates (20 and 40 L/h) were considered (*Sec. 4.2.3*).

3.2.3 Impact of Anolyte Flow Rates on COD Values

In addition to affect the process efficiency (*Sec. 4.1.4*), the wastewater flow rate directly impacted the purification level of the 1000-L MFC. Higher flow rates implied lower hydraulic retention times (HRT). Therefore, the treatment time of wastewater decreased, which altered COD removal efficiency and organic loads of effluents at the MFCs outlet (*Fig.21*).

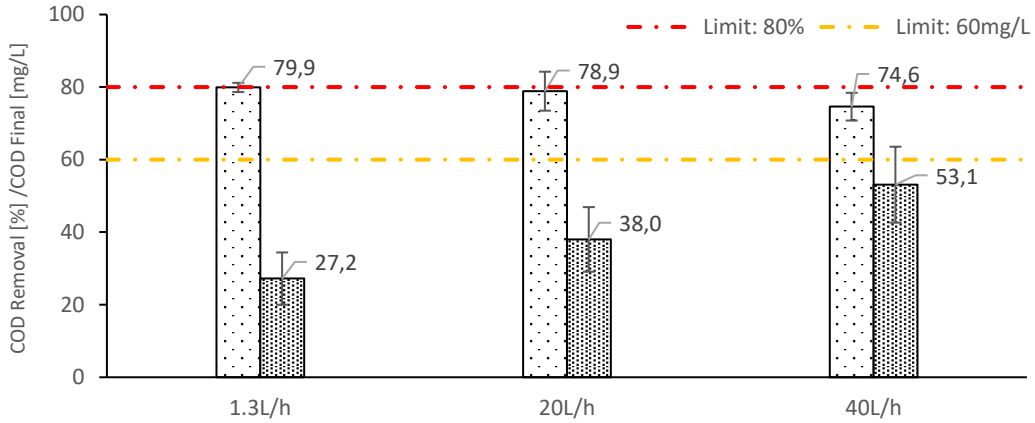

Figure 20: *Influence of wastewater flow rates on COD removal efficiencies (sparse dots) as well as effluent organic loads (compact dots) under the following conditions: $q_{an} = q_{cat} = 1.3$, 20 and 40 L/h, $P_{air} = 0.5$ bar and MPPT device. Regulations for small WWTP (< 10'000 PE) are displayed in red (removal efficiency) and orange (discharge concentration).*

Increasing the treating capacity of the 1000-L MFC by augmenting flow rate of treated influents impacted on both, COD removal efficiency and discharge concentration of organic matter. An augmentation of the anolyte flow rate decreased the removal efficiency and at the same time increased the residual organic load found after wastewater purification (*Fig.21*). With a treating speed of 20 L/h the values stayed within federal regulations (COD removal = 78.9 ± 5.4%, discharge concentration = 38.0 ± 8.9 mg/L). However, at 40 L/h the legislation was just barely not fulfilled. Values (including standard deviations) approached 78.4% for COD removal and 63.6 mg/L for residual organic load, approximatively 5% exceeding Swiss law for wastewater discharge. Due to the small deviation in regard to the legislation, the upper capacity limit of the MFC system was considered to be 40 L/h, which translated to a daily volume of 0.96 m^3. The treatable capacity could even be fixed to 1 m^3/day due to continual system performances improvement over time (*Sec. 4.4.3*).

Comparing with the values obtained in batch mode (*Tab.6*), the 1000-L MFC performance increased by a factor 6, passing from a daily treatable wastewater capacity of 0.16 m^3 to 0.96 m^3, corresponding to a hydraulic retention time of 11.6 h. The HRT of *Châteauneuf* biological process varies with weather conditions. During raining days the flow rate is maximal and the HRT minimal around 0.60 h. The WWTP average hydraulic retention time is 3.0 h, whereas in dry weather during the night it can reach as high as 8.6 h. To match this condition, the MFC installation should be able to treat 1.3 m^3 a day, which should be conceivable through process optimisation and design modifications.

Energy Generation: This chapter is partly confidential

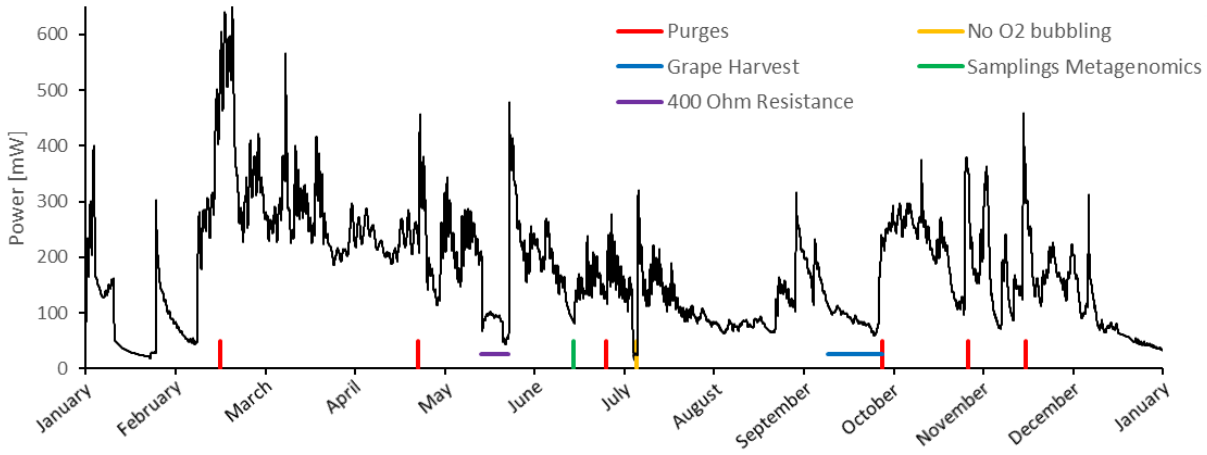

Figure 21: *Recorded power for the entire 1000-L MFC installation (addition of the power of each independent cart), over a year of operation [Jan.19 - Jan.20]. The different events happening during that period are displayed in the Figure.*

During purges, the anolyte of the 1000-L MFC was replaced with new wastewater from the primary clarifier of the WWTP in order to precipitate solid particles present in the MFC's anodic compartments. Purges were performed on the entire MFC-Stack and power pics were observed after each operation possibly due to higher organic matter concentrations (fresh medium) available to microorganisms.

Between May and June, the system was switched to 400 Ω resistances and generated power dropped before MPPT modules were re-established. The resulting power pic occurred due to the capacitor effect of MFCs, which self-stocked energy that was then released when MPPTs were reintroduced.

When no air was bubbled through the MFC's cathodes (July), power decreased 5.7 times (*Sec. 4.1.1*) because without oxygen as electron acceptor, the electron transfer from anodes to cathodes was hindered, hence less energy was produced.

The grape harvest period induced a reduction of the power generation due to the increase of the cell internal resistances (*Sec. 4.4.2.1*).

During electrode samplings, the electrical connections were partially disrupted which explained the power drop between June and July.

3.3 Independent Operating Variables

Because the 1000-L MFC was directly implemented in the WWTP of *Châteauneuf* to work under real conditions, some independent variables affected the process. These variables included among other things the wastewater composition as well as the microorganisms' population. All independent variables influencing the power generation are displayed on the following figure (*Fig.39*).

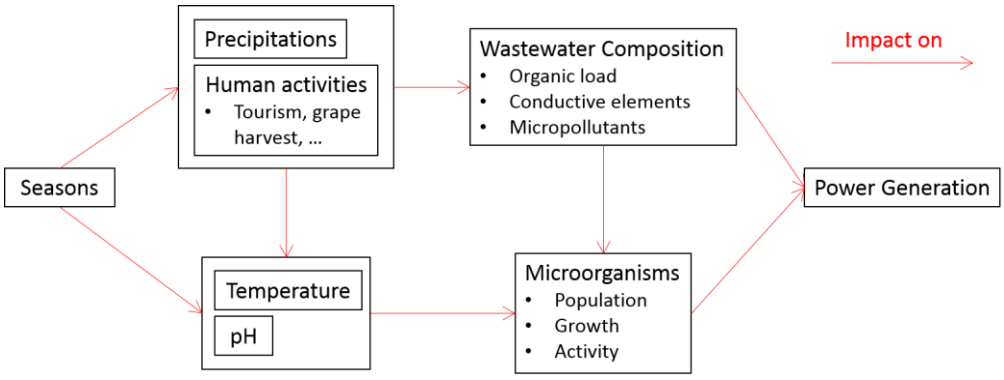

Figure 22: *Independent variables impacting power generation of the 1000-L MFC.*

One of the most important factors to consider when producing energy with MFC systems built for wastewater treatment is the constant change during the year when the reactor is in function. Indeed, the power output varies depending on the seasons (spring, summer, fall, winter), which affected the temperature and pH of the incoming wastewater (*Fig.40*) and the direct impact of rain falls and human activities.

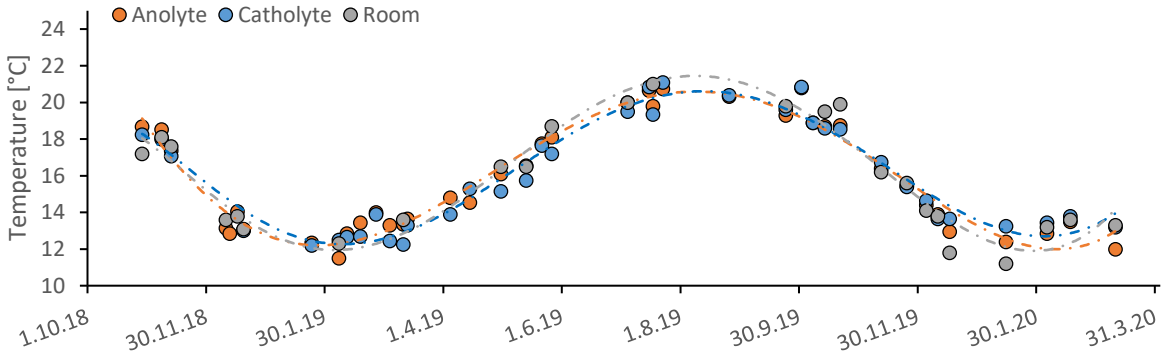

Figure 23: *Temperature profile for wastewater (anolyte), groundwater (catholyte) and air (room).*

The pH can affect the performance of the system by modifying the microorganisms' population [37], the electrochemical activity of the redox species in the microbial electron transfer chains [38] as well as the metabolic rate of the microorganisms [39]. The wastewater temperature can also affect the MFC because it influences the microbial metabolism [40]. It was shown that microorganisms in MFCs are more active at higher temperatures (20-30°C) [41] and confirmed by direct implementation of MFC systems on WWTPs [42,43]. Therefore, the 1000-L MFC was expected to be more efficient in the summer (> 20°C) than during the winter (12°C) [44].

The human activities and rain fall levels directly affect the wastewater composition, especially in terms of organic load that increased with important human activity and diminished with rain fall due to dilution. In addition to modify wastewater, these two variables also impact on its pH and temperature (*Fig.39*).

3.3.1 Organic Load and its Impact on Power Generation

The organic load (quantity of organic matter employed as substrate by the microorganisms) directly affected power generation with the 1000-L MFC as previously mentioned (*Sec. 4.3.3 & 4.4*). However, the organic load principally depended on two majors variables: the climatic conditions and human activities. When working under changing weather with rain falls, the wastewater at the inlet of the WWTP was diluted and organic matter concentrations (pollutants) was reduced what impacted the power output as shown in the subsequent figure (*Fig.41*). Here, power generation drastically decreased from 0.30 down to 0.14 W during the first strong rain fall event (days 1 to 5) and the same behaviour was observed during a second rainfall event, after 12 days (power decrease from 0.25 to 0.18 W). It was also possible to establish a link between human activities and power production with the MFC. Here, a sinusoidal curve was observed (*Fig.41*) with the maxima of each pics corresponding to the time span relative to intense human activities (between 8 and 20 o'clock), when organic matter is generated in notable quantities. The average power variance from day/night cycles was about 45 ± 17%. The power generated during weekends was less important as well, due to a more limited concentration of organic matter.

These data clearly demonstrated the dependency of power production from organic matter concentration that strongly varied with changing weather conditions and human activity.

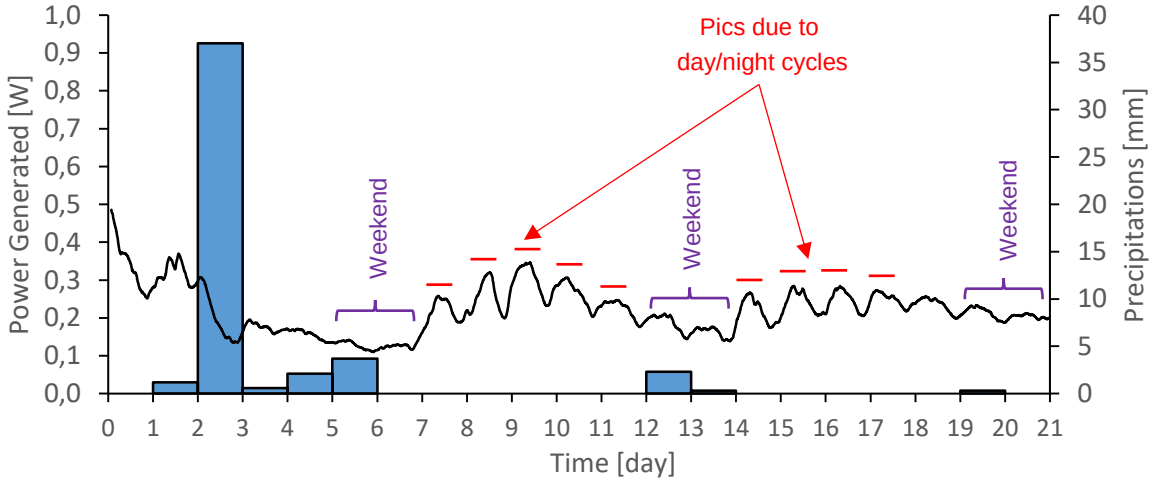

Figure 24: *Impact of climatic conditions (rain fall) and human activities (high organic load) on the power generated by the 1000-L MFC. The experimental conditions were the followings: q_{an} = 20 L/h, q_{cat} = 2.0 L/h with P_{air} = 0.5 bar. MPPT and charging devices during 3 weeks.*

3.3.2 Seasonal Effects

The different seasons had an important impact on the power generated by the 1000-L MFC. The concentration of organic matter was directly linked to the volume of wastewater to be treated. The observations effectuated, demonstrated that the daily volume of wastewater entering the WWTP was clearly higher during the summertime (June - August) with an average of 24'000 cubic meter of influents to be treated instead of 15'500 m^3/day for the rest of the year (*Fig.42A*), except for December 2019, where 23'000 m^3/day was recorded. As a consequence the organic matter available per volume in this period was much diluted (COD = 195 instead of 405 mg/L), what impacted on the power generation by the MFC as the influenct volume remained constant. At this point, power generated by the MFC dropped from 650 down to 350 mW (*Fig.42B*). At similar COD values, the progressive increase of power production between October 2018 and March 2019 referred to the growth and maturation of the microbial biofilm.

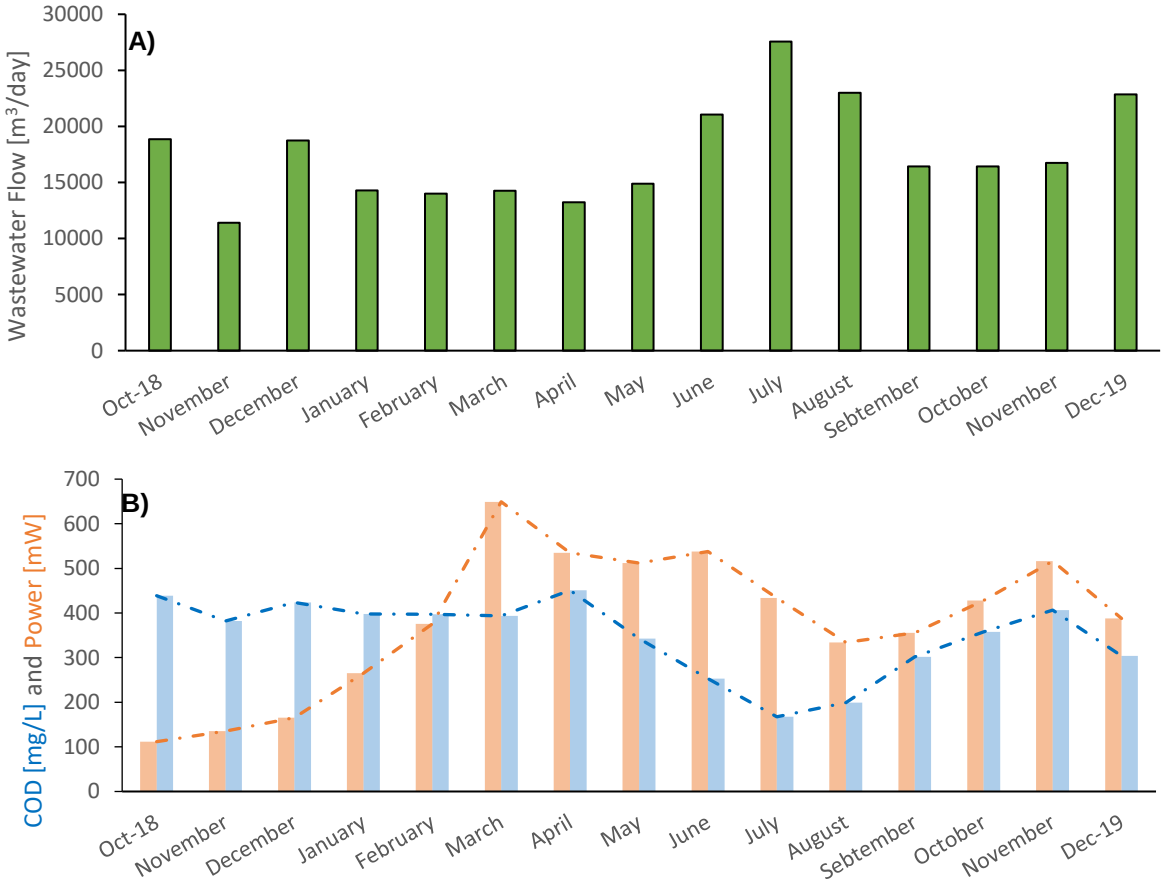

Figure 25: ***A)*** *Wastewater flow rates recorded by Châteauneuf WWTP.* ***B)*** *Impact of the organic matter concentration (blue curve) in wastewater and on generated power (orange curve). The power generation of the MFC installation was determined by polarisation experiments under the following conditions:* $q_{an} = q_{cat} = 40$ *L/h, with* $P_{air} = 0.5$ *bar and external variable resistances.*

3.3.2.1 Grape Harvest

The 2019 grape harvest was running between the 20th of September and 8th of October. During this period a drop in power generated by the 1000-L MFC was observed (*Fig.43A*). This decrease corresponded to a major augmentation of the internal resistance of the entire system (*Fig.43B*).

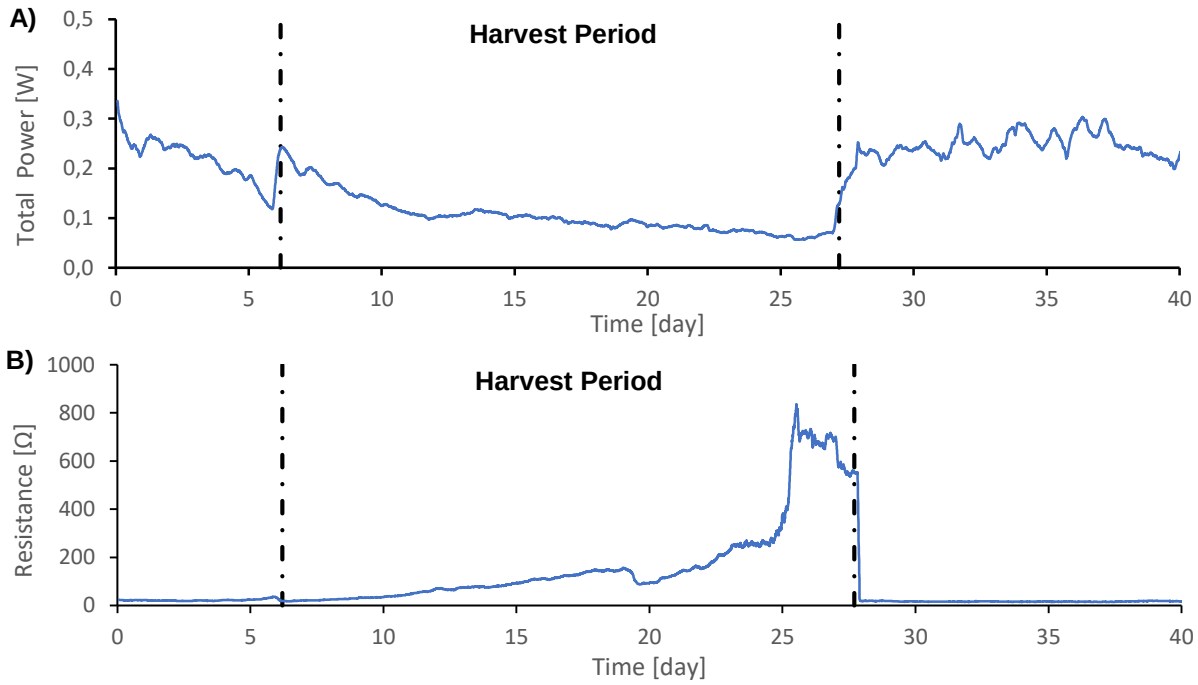

Figure 26: *Power generated by the entire 1000-L MFC (**A**) and average internal resistance (**B**) calculated for 40 days around the grape harvest period.*

Initially, at the beginning of the harvest, the power produced by the 1000 L-MFC installation instantly doubled from 0.12 to 0.24 W (*Fig.43A*). However, afterwards the latter constantly decreased down to 0.06 W (27th day). After that time, a system purge was performed, by replacing the anolyte with fresh wastewater, the power returned to the same level than previously observed (at the start of the harvest). In parallel, the average internal resistance increased from 20 to 550 Ω with a maximum value of 850 Ω (*Fig.43B*). The purge effect was radical with an immediate reduction of the system internal resistance down to an initial value of 20 Ω.

Wastewater COD, conductivity and pH were also analysed during the harvest period (*Tab.10*).

Parameters / Time	*t=0*	*t=12.7*	*t=20.0*	*t=27.0*	*Average*	*t=33.0*	*t=40.9*
COD inlet [mg/L]	137	68.7	173	154	**132**	326	264
Conductivity [µS/cm]	773	1197	1193	1075	**1155**	1338	1228
pH [-]	7.57	7.35	6.90	6.99	**7.13**	7.08	7.05

Table 7: *Key parameters for wastewater used as anolyte in the 1000-L MFC. The average referred to the data obtained during the grape harvest period (days: 12.7, 20.0 and 27.0).*

Surprisingly, the organic matter content during the grape harvest period was similar (*Tab.10*) to the one observed at the start of the experiment (t=0). In addition, a small decline of the pH was observed but no significant. The only parameter inclined to impact the power generation was the anolyte conductivity which increased by 50% from 773 to 1155 µS/cm. However, on the contrary, a reduction of the power produced by the 1000-L MFC installation was observed (*Fig.43A*). The power generation was linked to the internal resistance of the system. A higher resistance implied a lower production of energy. One possible explanation was the accumulation of solid suspended particles in the anodic compartments, which negatively impact cell resistance. This hypothesis was comforted by the visual observation of "murkier" wastewater at the system inlet during the grape harvest period, which was not the case for the rest of the year. The contrast was particularly visible for the 3rd and 4th carts (*Fig.44*).

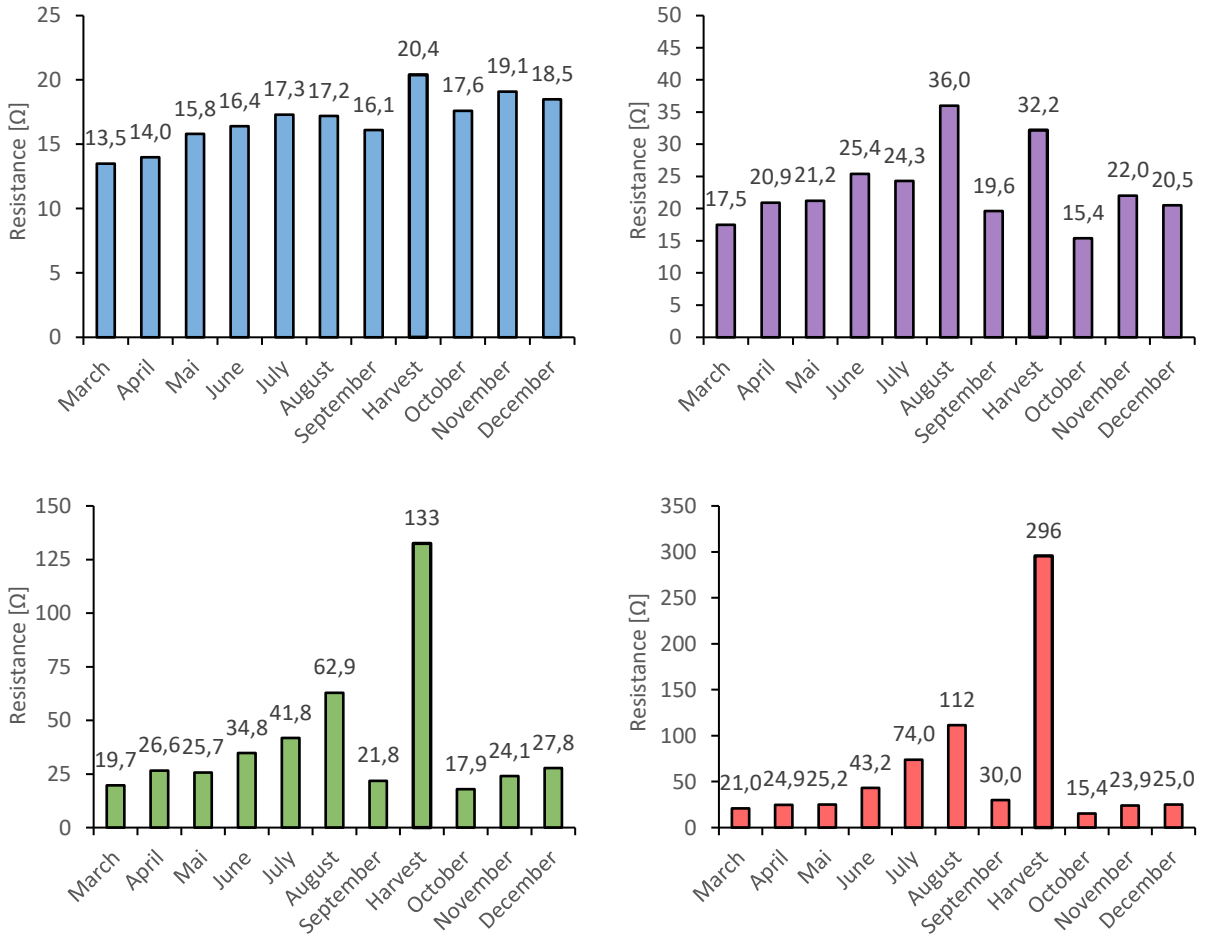

Figure 27: *Internal resistance for the different cart of the 1000-L MFC over time. The experimental conditions were the followings:* q_{an} *= 20 L/h,* q_{cat} *= 2.0 L/h with* P_{air} *= 0.5 bar and MPPT use.*

3.3.3 Microorganisms' Impact on Power Generation

In addition to the temperature, pH and organic matter concentration of wastewater, the power generated by the MFC-installation was also affected by the microbial biofilm formed on anodic electrodes. The composition of this biofilm directly impacted power generation properties. A higher proportion of exoelectrogenic microorganisms increased energy output. Moreover, as the biofilm matured over time due to microorganisms' growth, power rose in this regard.

3.3.3.1 Microbial Community

Before looking into the different microorganisms present on the anodes, a quantification relative to the amount of DNA extract per square centimetre of electrode was performed. The results of this analysis were displayed in the following graph (*Fig.45*).

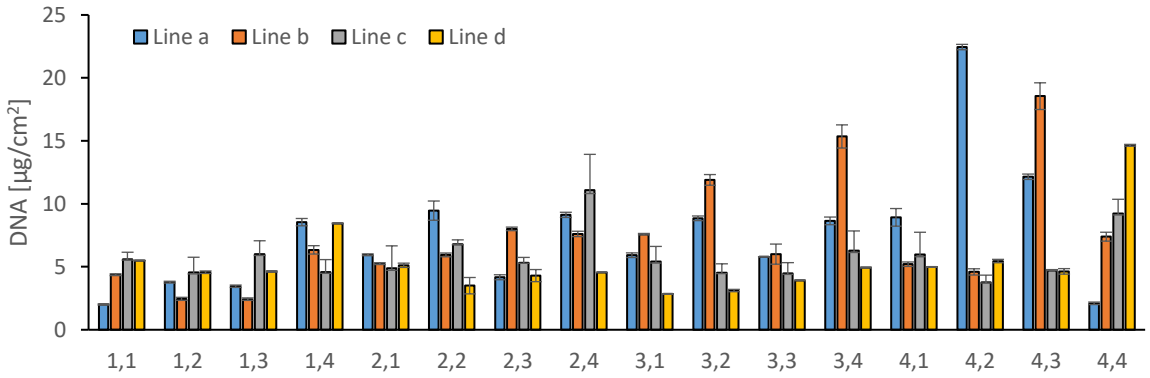

Figure 28: *Amount of DNA extract per anodic surface as a function of electrode position inside the 1000-L microbial fuel cell.*

An average amount of 6.54 µgram of DNA was extracted per cm² of electrode (*Tab.11*). A slight difference was observed when comparing the lines between themselves. From line a to d the quantity of DNA extract somewhat diminished from 7.58 to 5.32 µg/cm², passing by 7.44 and 5.83 µg/cm² for line b and c, respectively. Therefore, the electrodes of line a and b were composed with higher concentrations of microorganisms than the electrodes of the 2 other lines.

Parameters	*Cart 1*	*Cart 2*	*Cart 3*	*Cart 4*	***Average***
Line a	4.45	7.18	7.30	11.41	**7.58**
Line b	3.90	6.70	10.2	8.94	**7.44**
Line c	5.18	7.03	5.18	5.92	**5.83**
Line d	5.78	4.37	3.70	7.43	**5.32**
Average	**4.83**	**6.32**	**6.60**	**8.42**	**6.54**

Table 8: *Average DNA extracted in µgram per cm² of RVC anode for each line and cart of the 1000-L MFC.*

The same trend was observed when comparing the different carts. There were more microorganisms (+74%) on the electrodes with the last cart (8.42 µg/cm²) than the first one (4.83 µg/cm²) (*Tab.11*). This observation was intriguing because wastewater entering within the last cart was less concentrated in organic matter and, therefore, less substrate was present for microorganisms' growth, which would tend to imply that less organisms could mature at the outlet.

DNA extractions were also performed on the first and last cathodic electrodes of all treatment line to understand which microorganisms developed under aerobic conditions on the cathodes (*Fig.46*). A sizable quantity of microorganisms were present at the system's inlet (12.3 µg/cm² on average), whereas a much lower amount at the installation outlet (2.15 µg/cm² on average). The microorganisms were naturally present within the groundwater source and seemed to grow directly at the entrance of the 1000-L MFC.

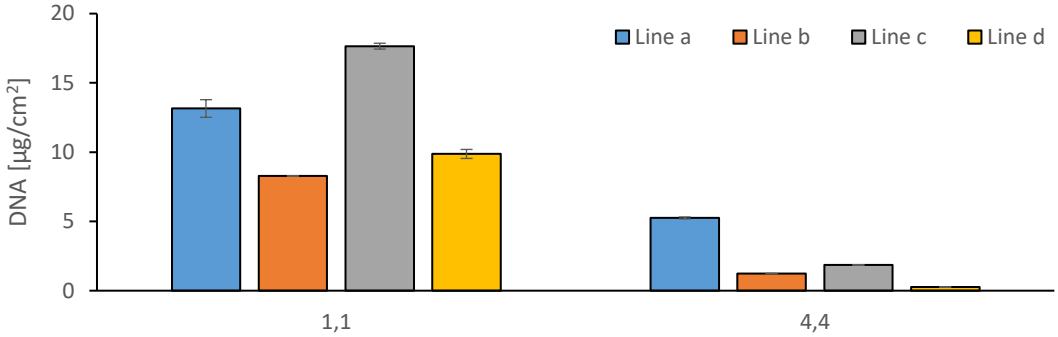

Figure 29: *DNA extracts per cathodic surface as function of electrode position inside the 1000-L microbial fuel cell.*

For the first microbial fuel cells of each treatment line (*Fig.47A*), the quantity of DNA extracted from cathodes (12.2 µg/cm²) was 2.8 times higher than the extractions realised from anodes (4.36 µg/cm²). On the contrary, for the last cells (*Fig.47B*) there were 3.9 time less DNA on cathodes (2.15 µg/cm²) than on anodes (8.34 µg/cm²).

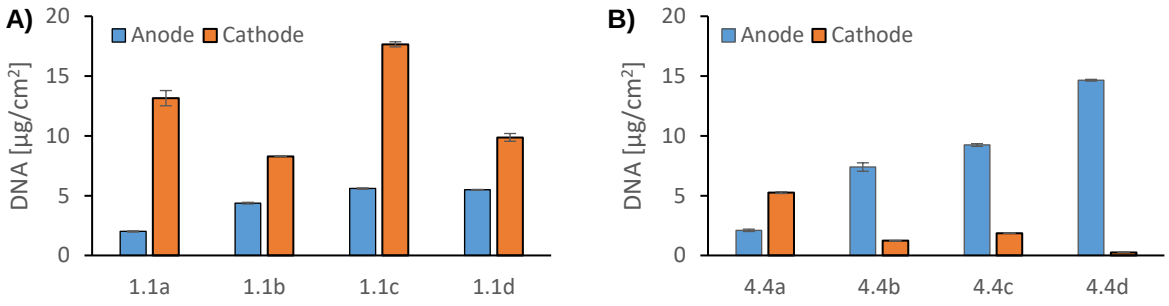

Figure 30: *Comparison between the quantities of DNA extracted per anodic and cathodic surface for the first (**A**) and last (**B**) cell of the 1000-L MFC.*

3.3.3.2 Microorganisms' Growth and Activity

As the microorganism's growth impacts on recoverable energy from the process, it was possible to characterise the biofilm maturity by performing polarisation experiments (*Sec. 3.4*). The slope of the polarisation curve (*Fig.48A*) permitted deducing the internal resistance of the cell, whereas the summit of the power curve (*Fig.48B*) allowed founding the maximal power generated by the system as well as the current at that point. Next charts (*Fig.48*) present the best polarisation results relative to the first cart of the 1000 L-MFC installation.

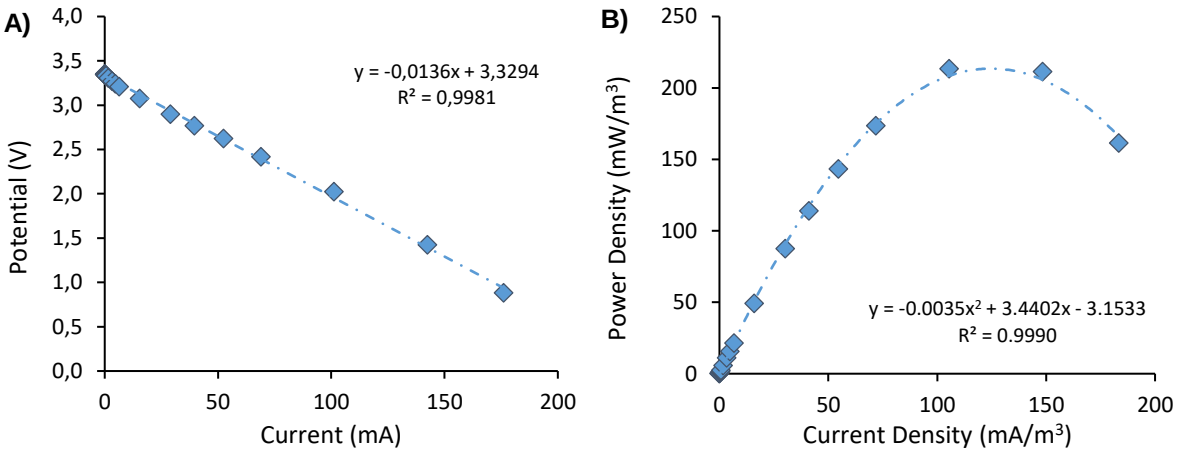

Figure 31: *Polarisation (**A**) and power (**B**) curves for the first cart of the 1000-L MFC obtained with a biofilm maturity of 0.5 year. The experimental conditions were the followings: $q_{an} = q_{cat} = 40$ L/h, with $P_{air} = 0.5$ bar and a resistance box used for manual external load variations.*

The best recorded values of power and current densities are listed in the subsequent table (*Tab.12*).

Power Density [W/m³]	Current Density [A/m³]	Internal Resistance [Ω]
0.21	0.12	14.1

Table 9: *Electrochemical parameters (Sec. 3.4) calculated from figure 48.*

The power and current generated during the process as well as the system internal electrical resistance were all essential bioelectrochemical parameters used to assess the microbial growth evolution over time. By representing the evolution of the power (in terms of absolute values) delivered by the 1000L MFC through time as a function of the external resistance (*Fig.49*), it appeared that the power generated by the system slightly increased from 95 up to 145 mW within 6 weeks. During this period, the microbial biofilm grew and did not produce significant amounts of energy. However, after this 6-weeks acclimatisation period, more and more energy was produced with a maximal value of 650 mW after half a year of processing (*Fig.49*), corresponding to a relative increase of 580% from the initial step (week 1). During the production period (weeks 7 to 23), a stable biofilm formed. The energy delivered by the

microorganisms and harvest by the installation increased due to two different factors. Firstly, as more microorganisms were present the energy output was higher. Secondly, with a stable biofilm the microorganisms switched from their growing phase to production and did not consume as much energy as in the acclimation period. After 7 months of processing, the energy generation dropped and stabilised at 500 ± 50 mW, except for weeks 48 (355 mW) and 62 (390 mW). This reduction could be explained because less organic matter was available at the time (*Sec. 4.4.2*) and the hypothesis was that with a limited amount of substrate the microorganisms might switch their metabolism to endogenous respiration where they oxidised some of their own cellular mass instead of new organic matter absorbed from wastewater.

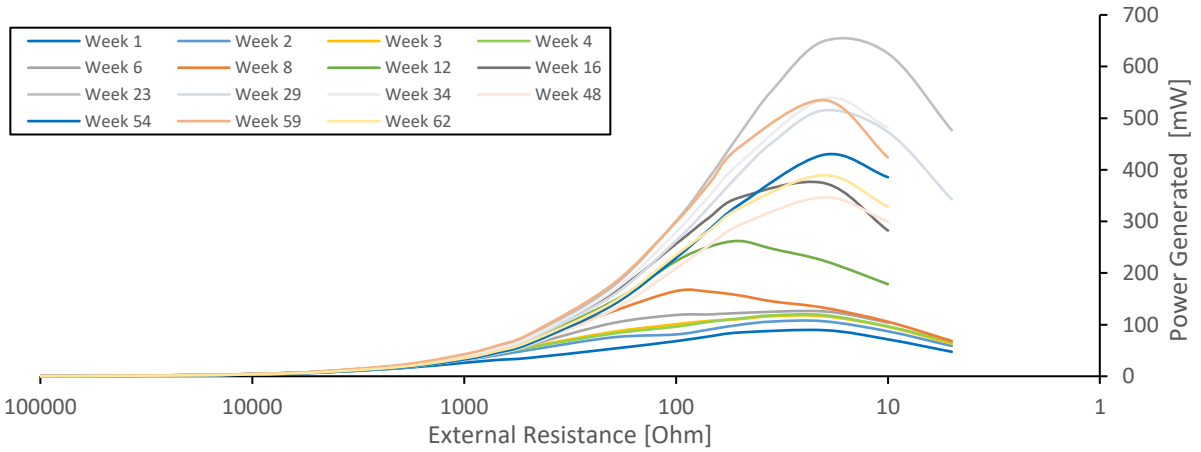

Figure 32: *Evolution of the absolute power generated with the 1000-L MFC as a function of external electrical resistances, monitored during a 62-weeks period. A maximum of 650 mW was achieved at an average internal resistance of 16 Ω.The experimental conditions were the followings:* $q_{an} = q_{cat} = 40$ *L/h, with* $P_{air} = 0.5$ *bar and resistance boxes used for manual external load variations.*

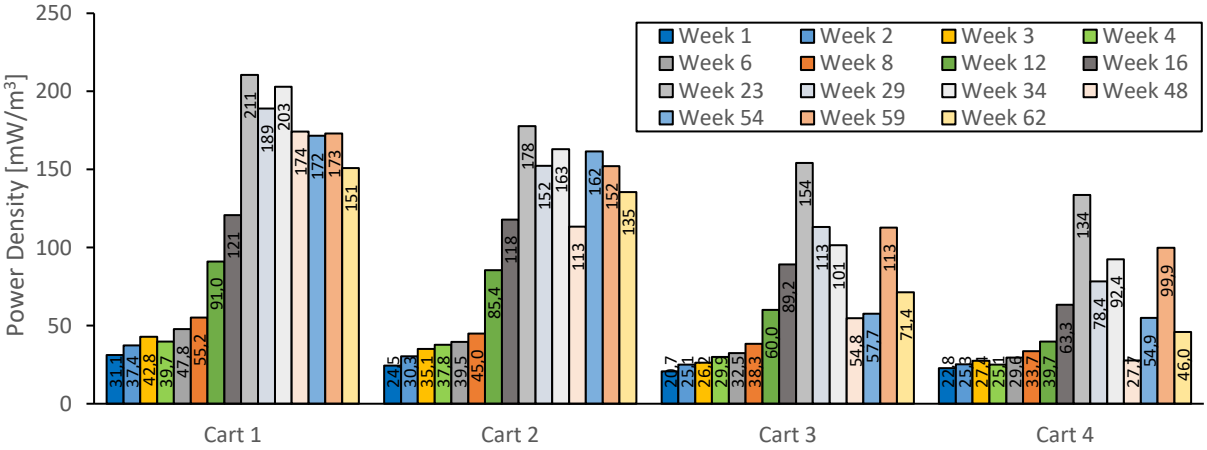

Figure 33: *Power density reached by each individual cart of the MFC scale-up installation as function of time (from week 1 to 62). The experimental conditions were the followings:* $q_{an} = q_{cat} = 40$ *L/h, with Pair = 0.5 bar and resistance boxes used for manual external load variations.*

Water and wastewater were introduced to the first cart of the 1000 L-MFC installation and then passed thought cart n° 2 and 3 before entering the fourth cart and leaving the reactor. Therefore, more nutriments (organic matter) were present at the reactor entrance and higher power (*Fig.50*) and current densities (*Fig.51*) were achieved in comparison to the next carts (cart 2 to 4). The internal resistance was also lower in the first cart (*Fig.52*).

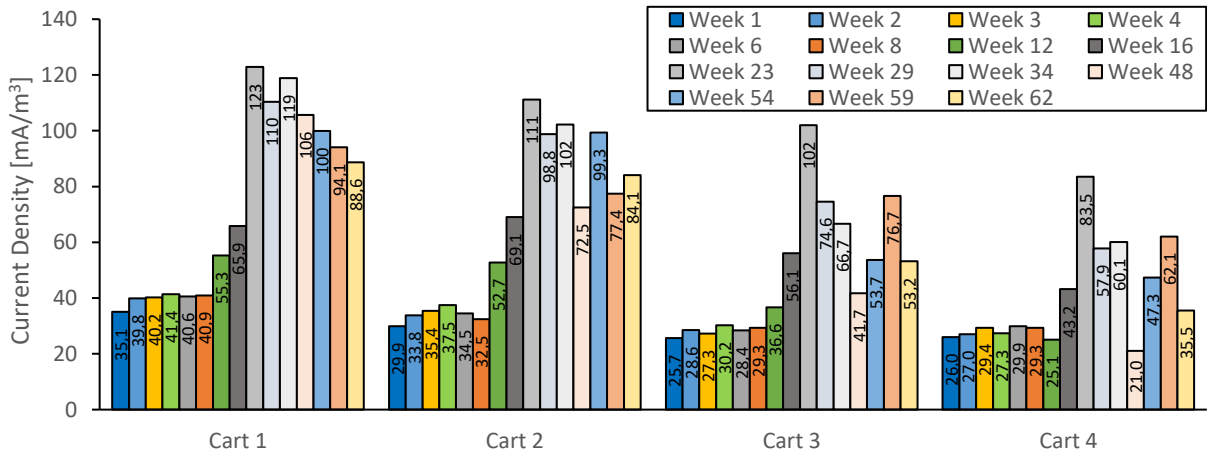

Figure 34: *Current density reached by each individual cart of the MFC scale-up reactor as function of time (from week 1 to 62). The experimental conditions were the followings: q_{an} = q_{cat} = 40 L/h, with Pair = 0.5 bar and resistance boxes used for manual external load variations.*

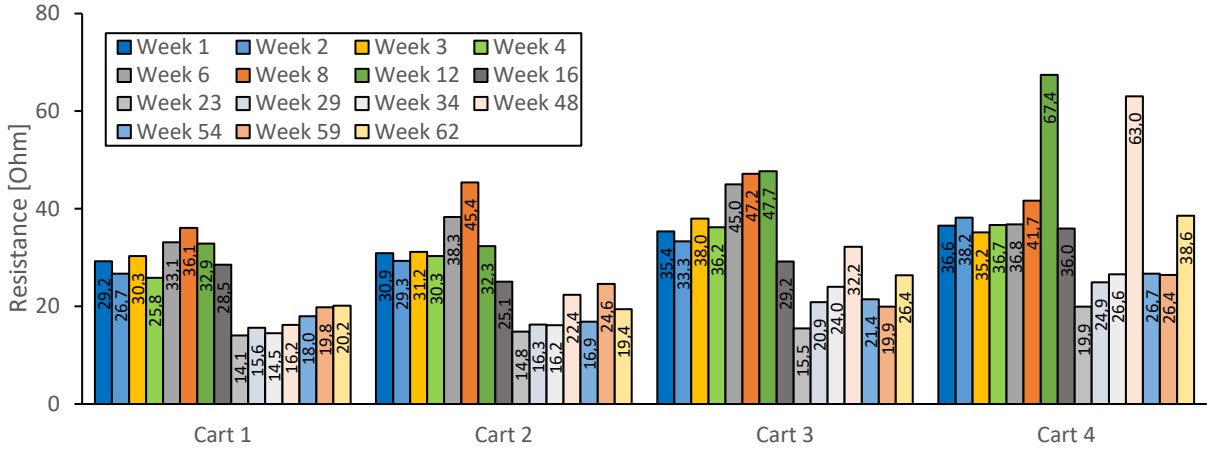

Figure 35: *Internal resistance of each individual cart of the MFC scale-up installation as function of time (from week 1 to 62). The experimental conditions were the followings: q_{an} = q_{cat} = 40 L/h, with Pair = 0.5 bar and resistance boxes used for manual external load variations.*

Comparatively, the normalised power generated by the 1000-L MFC (500 mW/m³, *Fig.5*) was on average 35% higher than the one produced with the prototype (370 mW/m³, *Fig.4*). In the ideal case scenario using potassium ferricyanide (to boost the system) a power generation of 1100 mW/m³ was obtained with the prototype (*Sec. 7.3G*), defining the upper limit of our MFCs for power generation.

3.3.3.3 Microorganisms' Population

To determine the microorganism population on anodes and cathodes of the 1000-L MFC, a metagenomics analysis was performed (*Sec. 3.9*). The microorganisms' population was determined at different positions for each treatment line (*Fig.13*).

To facilitate the analysis, only the top five phyla were taken into consideration, accounting for ~95% of the total detected microbiome. The other less important phyla were regrouped together and classified under the appellation "*Other*". This investigation was performed for both anodic and cathodic electrodes (*Fig.53*).

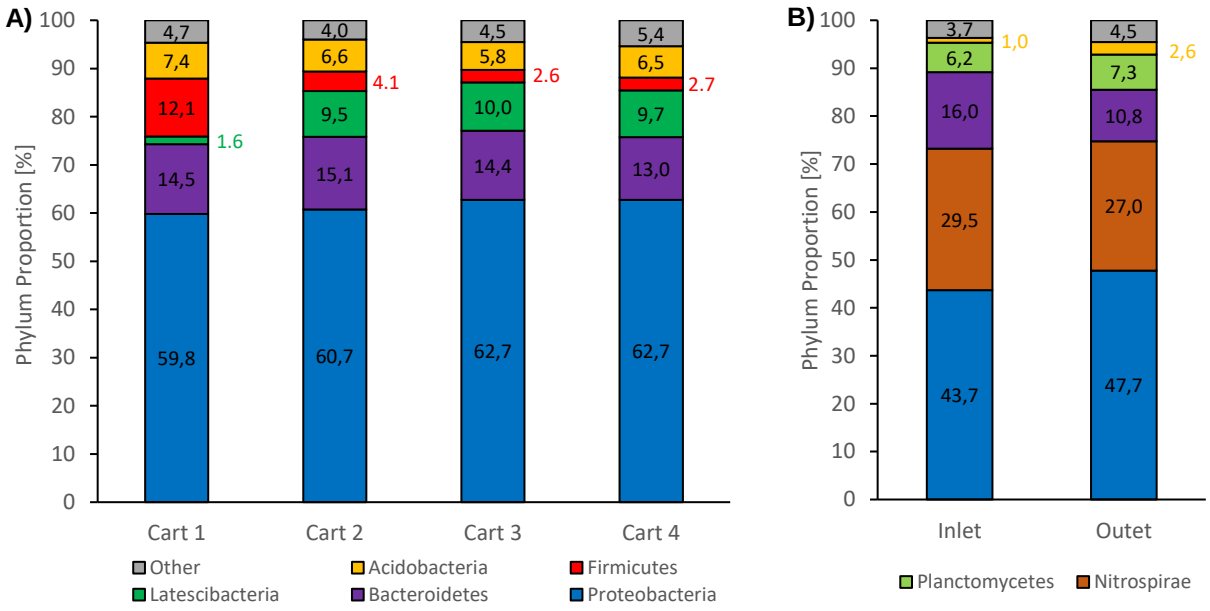

Figure 36: *Identified microbiome at the phylum level for anodes (**A**) and cathodes (**B**) of the 1000-L MFC . For the anodes, the analysis was performed for each cart (MFC electrodes of the same cart were treated as a whole and displayed as "Cart 1-4"). For the cathodes, 4 samples were taken at the inlet and outlet of the MFC (Fig.13: electrodes 1.1 a-d and 4.4 a-d).*

The anodic phyla (*Fig.53A*) were *Proteobacteria* (61.5% as average value), *Bacteroidetes* (14.2%), *Latescibacteria* (7.7%), *Acidobacteria* (6.6%) and *Firmicutes* (5.4%). Except for *Latescibacteria* (including fermentative type microorganisms), all of the detected phyla are known to contain populations of exoelectrogenic bacteria [45].

The cathodic phyla (*Fig.53B*) showed some similarities but also differences relative to the microbiome composition. In this case, *Latescibacteria* and *Firmicutes* were replaced by *Nitrospirae* (28.3%) and *Planctomycetes* (6.8%) phyla. *Proteobacteria* phylum was also less abundant (45.7%). *Nitrospirae* is a phylum involved in the nitrification of N-species, whereas *Planctomycetes* a phylum of aquatic bacteria.

Another interesting observation is the evolution of the proportion of identified phyla relative to the position thought each wastewater treatment line. For instance, very few *Latescibacteria* were found on the anodic electrodes of the first cart, whereas up to 13.4% were discovered on the last one (*Fig.54A*).

For *Firmicutes* it was the opposite; at the reactor inlet, up to 16.8% bacteria of that phylum were observed, whereas only around 1.5% were present on the electrodes of the 4th cart (*Fig.54B*).

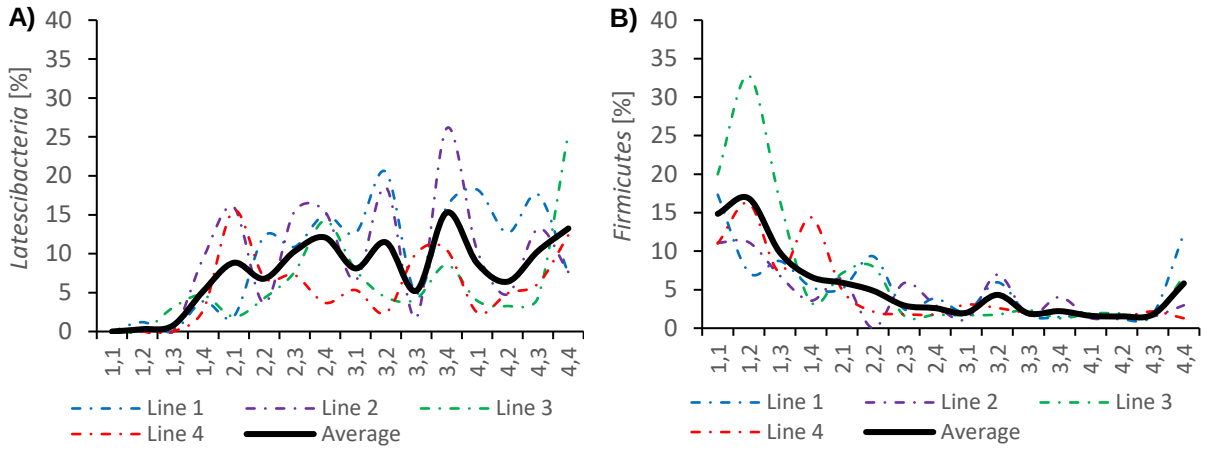

Figure 37: *Proportion of Latescibacteria (**A**) and Firmicutes (**B**) on anodic electrodes as function of the sampling position in each treatment line (1-4). An average tacking into account the 4 treatment lines was established as mean of comparison.*

Proteobacteria, Bacteroidetes and *Acidobacteria* anodic phyla were steady for all treatment lines. In addition, there was no difference in the cathodic microbiome composition between system inlet and outlet.

At the genus level, there was more the 130 different identified genus. To simplify the investigation, the genus were classified into 7 categories, each representing a specific bacteria function. These category were referenced as follow (the classification details are displayed under the annex section (*Sec. 8.3H*)):

1. *Exoelectrogen*: for all bacteria transferring electrons extracellularly.
2. *Denitrification*: for all bacteria reducing N-species.
3. *Nitrification*: for all bacteria oxidizing N-species.
4. *Fermentative*: for all bacteria producing, through fermentation, end-product such as CO_2, H_2 or acetic acid for instance.
5. *Desulfurization*: for all bacteria reducing S-species.
6. *Unclassified*: for all bacteria with no precis classification (no information relative to the above-mentioned categories 1 to 5)
7. *Other*: for all uncultured bacteria and bacteria with no metagenomic data at the genus level.

The following chart (*Fig.55*) displays the proportion of each bacteria type for both anode and cathode electrodes.

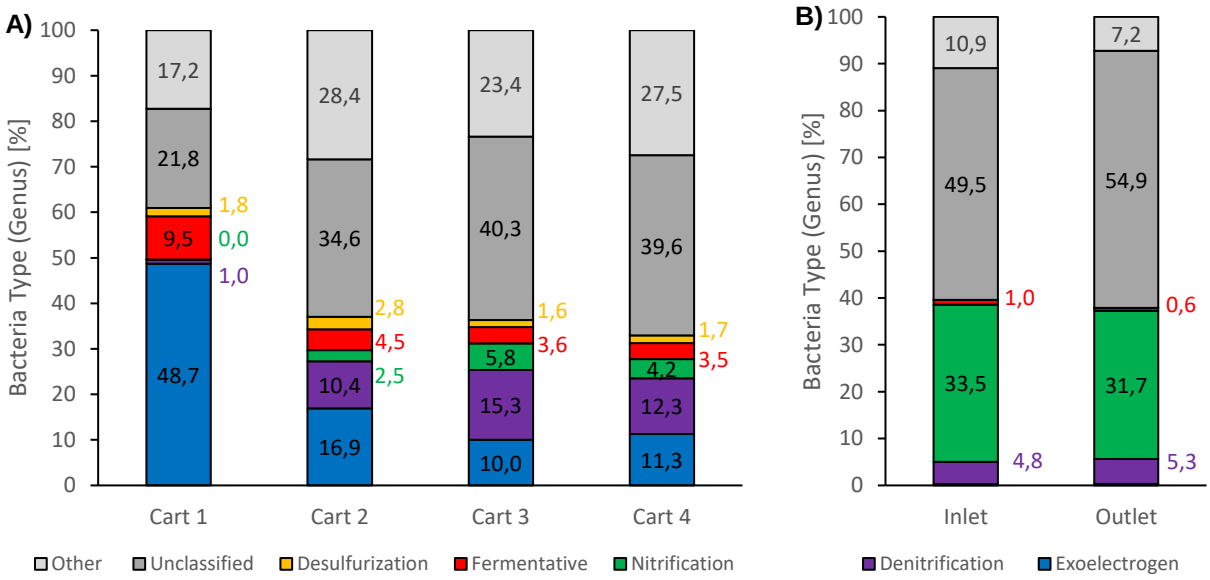

Figure 38: *Bacteria type according to genus classification (Sec. 8.3H) for anodes (**A**) and cathodes (**B**) of the 1000-L MFC. For the anodes, the analysis was performed for each cart (MFC electrodes of the same cart were treated as a whole and displayed as "Cart 1-4"). For the cathodes, 4 samples were taken at the inlet and outlet of the MFC (Fig.13: electrodes 1.1 a-d and 4.4 a-d).*

Exoelectrogenic bacteria were abundantly present (48.7%) on anodic electrodes of the first cart of the 1000-L MFC (*Fig.55A*). Then, the proportion of bacteria dropped to 17% for the second cart and stabilised around 10% for carts 3 and 4. This observation was in accordance to recorded electronic data indicating a higher power generation in the first cart (*Secs. 4.3.3* and *4.4.3.2*), where organic loads were higher. Therefore, one could assume that a higher content of organic matter allowed the exoelectrogenic community to develop more consequently and because of the exoelectrogenic biofilm and substrate were more significant, more energy could be produced in comparison to the other carts.

No exoelectrogens were found on cathodic electrodes (*Fig.55B*). Some fermentative (< 10%) and desulfurization (< 3%) type bacteria were present on anodic electrodes but quasi-absent on cathodic ones. Both electrode types were covered by denitrifying bacteria, from 10 to 15% for the anodes of carts 2-4 (only 1% for cart 1 because here exoelectrogens were more abundant) and around 5% on cathodes. The cathodic electrodes were populated by nitrifying bacteria with up to 33.5%, whereas the proportion on the anodes was less consequent (5.8% at the maximum). The fact that nitrifying and denitrifying bacteria were found, indicated the potential denitrification capacity of the 1000-L MFC as mentioned under the next section (*Sec. 4.5.2*).

Most of the exoelectrogenic bacteria discovered on the anodes were part of the *Geobacter* genus (81.8%, *Fig.56*). Other significant bacteria were *Desulfobulbus* (4.3%), *Macellibacteroides* (4.0%), *Desulfovibrio* (3.4%), *Clostridium* (1.7%) and *Paludibacter* (1.0%). All of them transferred electrons, generated by their metabolisms during the oxidation of the organic matter, to the electrodes where they were attached and, thus, participate to the production of energy from wastewater. The large quantities of *Geobacter* was very much in line what others have reported about MFCs in Wastewater-MFCs. They are considered of the best electrogens one can have according to current knowledge.

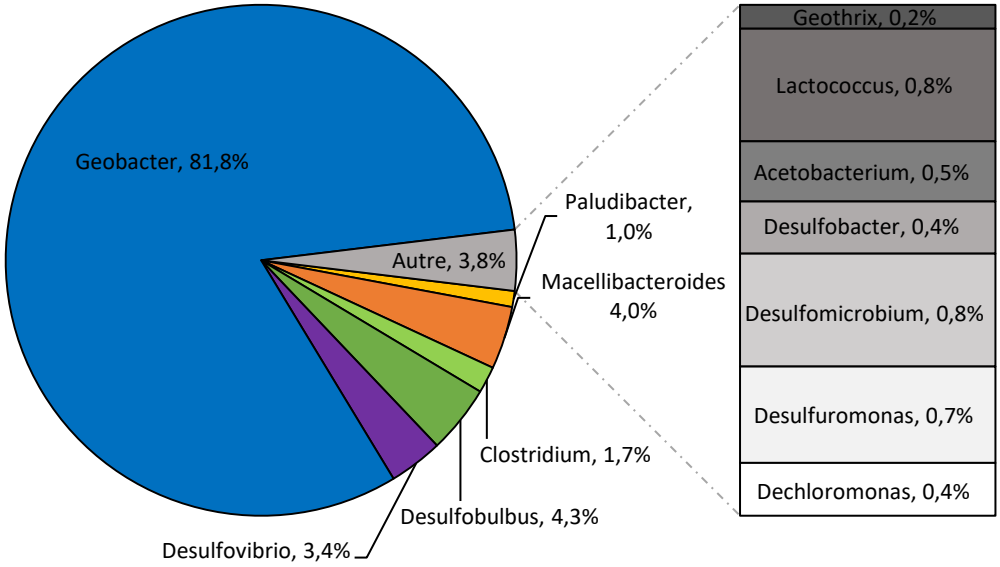

Figure 39: *Exoelectrogens (genus) repartition on anodic electrodes (average of 16 anodes) present on the first cart of the 1000-L MFC (Fig.55A).*

The proportion of exoelectrogenic bacteria declinedd in relation with the number of MFCs present in a wastewater treatment line. On the anodes of the first MFC (*Fig.57*, 1.1) more than half (58.4%) of the detected population of microorganisms were considered exoelectrogens. This value dropped to 39.0% after the last unit of the first cart (1.4) and stabilised around 10% at the outlet of the second cart (2.4), remaining constant until the end of the treatment line (4.4). A concentration gradient was also observed when analysing the organic matter content of a treatment line (*Sec. 4.3.3*), where the organic load declined from 228 mg/L (system inlet, 1.1) to 54.7 mg/L after the first cart (1.4), down to 50.0 mg/L after the 16th MFC unit (4.4). Thus, a possible correlation between the concentration of the organic matter in the anolyte and the amount of exoelectrogens constituting the anodic biofilm could be assumed.

Denitrifying and nitrifying bacteria were increasingly present between the inlet and outlet of each treatment line, whereas fermentative microbes tended to decline. Desulfurization type micobes remained stable in they population density. In addition, there was no difference in the cathodic microbiome composition at the genus level.

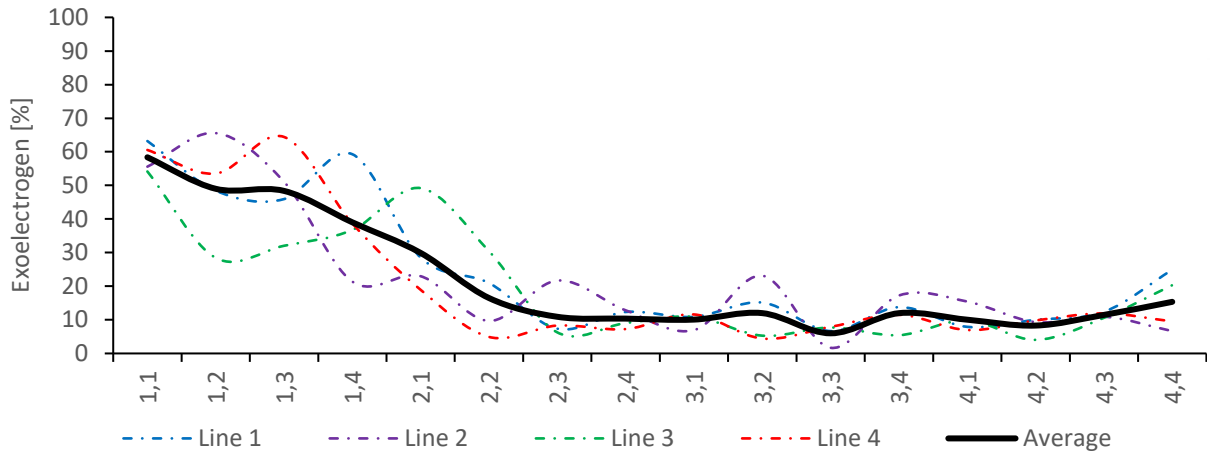

Figure 40: *Proportion of exoelectrogenic bacteria on anodic electrodes as a function of the sampling position in each treatment line (1-4). An average tacking into account the 4 treatment lines was established as mean of comparison.*

The observation of the operational taxonomic unit (OTU) as a function of the cell position in wastewater treatment lines indicated a clear decrease in the abundance of detected species from the inlet (cell 1) to the outlet (cell 16) of the 1000-L MFC (*Fig.58*). Average OTU for each cart confirmed that trend with a consistent drop of around 3'500-4'000 OTUs between the different carts (cart 1 to 4: 29'000 → 25'000 → 21'500 → 17'500 OTUs). This finding, in addition to the performed DNA quantification (*Sec.4.4.3.1*), demonstrated that DNA concentrations increased the further from the inlet (*Tab.11*), indicated that a high microbial diversity [46] was found at the system inlet, whereas at the outlet more specific microorganisms developed (less diversity but higher DNA mass content).

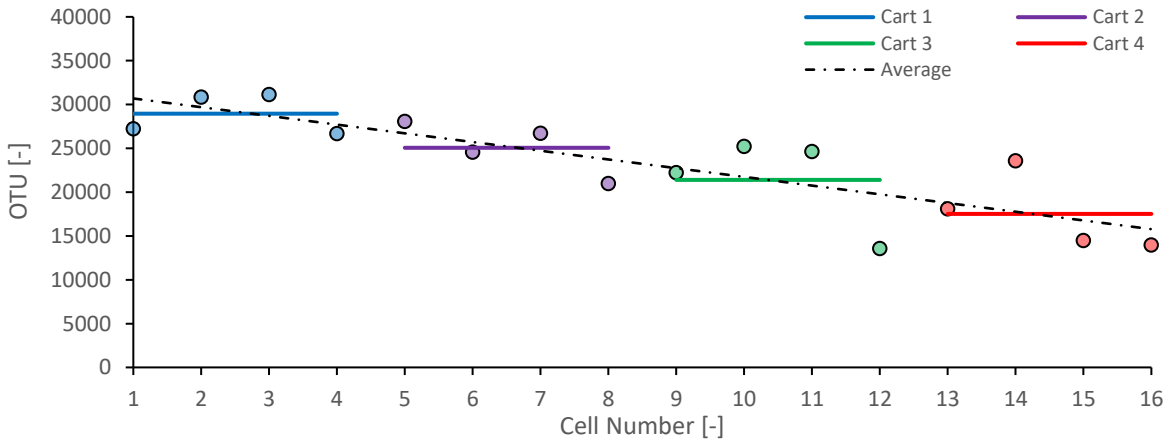

Figure 41: Operational taxonomic unit *(mean between treatment lines a to d) as a function of anodes location in the treatment line. An average value was also calculated for each cart.*

3.4 Mass Balance for the MFC system

A mass balance was established in order to understand the principal fluxes of elements within the 1000-L MFC. Solute elemental species were determined by ICP-OES (*Sec. 3.8*), whereas nitrogen compounds were quantified using spectrometry (*Sec. 3.10*). Micropollutants analysis were performed by ENVILAB SA using liquid chromatography-mass spectroscopy (LC-MS/MS) method.

3.4.1 Elemental Species Investigation

Prior to the investigation of the different solute fluxes within the MFC installation, an ICP-OES elemental screening was performed to determine the quantities of the major species present in wastewater. The result of that superficial analysis was displayed in the following table (*Tab.13*):

Element	***B***	***Ba***	***Ca***	***Fe***	***K***	***Mg***	***Mn***	***Na***	***Ni***	***P***	***S***	***Si***	***Sr***	***Zn***
[mg/L]	0.11 ± 38%	0.01 ± 14%	58.8 ± 11%	0.10 ± 40%	8.18 ± 26%	14.6 ± 7.7%	0.04 ± 54%	17.4 ± 4.3%	0.60 ± 6.6%	0.59 ± 4.7%	11.6 ± 3.7%	1.70 ± 23%	0.57 ± 15%	0.09 ± 25%

Table 10: *Elements detected in wastewater using ICP-OES screening.*

The migration of charged species is related to their concentration. The most concentrated ones easily migrate, whereas negligible fluxes occur for less concentrated species. In that optic, only major cationic species such as Ca (58.8 mg/L), K (8.18 mg/L), Mg (14.6 mg/L) and Na (17.4 mg/L) were thoroughly investigated. Sulphur (S) was also taken into consideration due to its high concentration (11.6 mg/L). Two other elements (Fe and P) were of interest. Phosphorus because the legislation fixes a limit value (< 0.8 mg/L) [35] for that element regarding treated wastewater discharge into lakes and rivers. Iron because it is used, under the form of $FeCl_2$ or $FeCl_3$, to remove soluble ortho-phosphate by precipitation [47] in order to avoid eutrophication lakes and rivers [48]. The concentration of phosphorus in the effluents was within the legal requirements (0.59 mg/L) because iron (III) chloride was added upstream of the 1000-L MFC. Iron present in the resulting wastewater entering the MFC system (0.10 mg/L) was related to the excess that did not react to precipitate phosphate into strengite ($FePO_4 \cdot 2H_2O$), vivianite ($Fe_3(PO_4)_2 \cdot 8H_2O$) or other iron phosphate species [49].

Precise ICP-OES quantifications were performed for above-mentioned elemental species based on AAS standards ($CaCO_3$, KNO_3, Mg metal, Na_2CO_3 and H_2SO_4) prepared with a 2% HNO_3 trace select solution. The elemental analysis were done in duplicate with samples collected during two experiments realised under the same operating conditions. Moreover, 2 to 3 sets of samples were gathered (at different dates) for each experiment to have a representative view relative to the migration of each species. The samples were collected at the inlet and outlet of the 1000-L MFC for both anolyte (wastewater) and catholyte (groundwater).

Next Figure (*Fig.59*) displays the average (experiments 10 and 11) elemental concentration of calcium, potassium, magnesium, sodium and sulphur within the anolyte and catholyte at the inlet and outlet of the MFC installation.

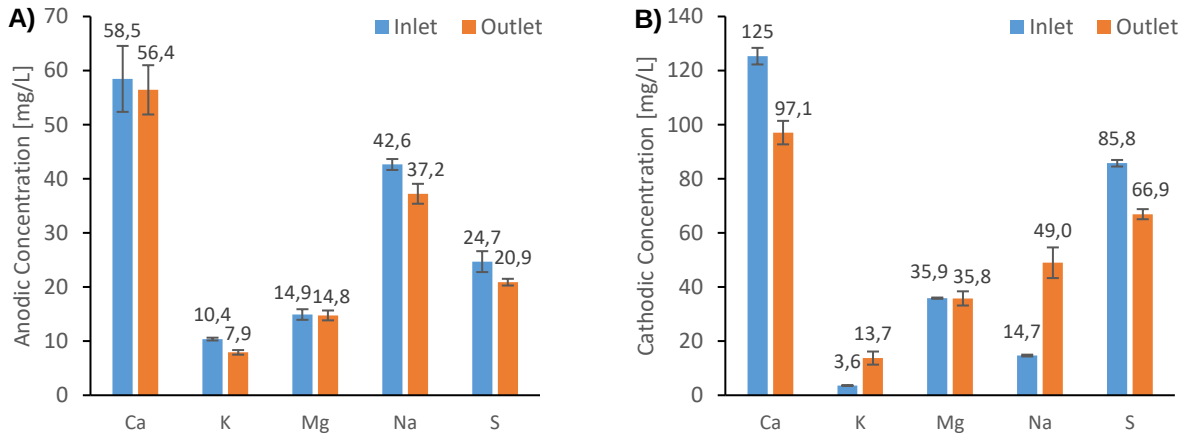

Figure 42: *ICP-OES quantification of calcium (Ca), potassium (K), magnesium (Mg), sodium (Na) and sulphur (S) for anolyte (**A**) and catholyte (**B**) under the following conditions: q_{an} = 20 L/h, q_{cat} = 2.0 L/h with P_{air} = 0.5 bar and MPPT device as storing modules.*

The concentration of each element within wastewater decreased when passing from the inlet to the outlet of the MFC-installation (*Fig.59A*). For instance, sodium dropped from 42.6 to 37.2 mg/L. This reduction was explained by the fact that positive species migrated thought the VANADion™ membrane to maintain the electroneutrality of the system. Indeed, the transfer of electrons to the cathode during the energy harvesting process engendered an excess of negative charges within that compartment and cationic species, thus, migrated from anode to cathode to compensate for that excess. Therefore, the concentration of each species within groundwater should increase (*Fig.59B*). This was the case for potassium (+280%) and sodium (+230%) while magnesium remained stable (-0.28%). However, a reduction of the concentration of calcium (-22.3%) and sulphur (-22.0%) was observed. This diminution could only be explained by the fact that these species either precipitated and formed solid compounds or left in an unknown fashion. Most probable cathodic precipitates might include [50]: $CaCO_3$ (sol. = 6.6 mg/L), $Ca_3(PO_4)_2$ (sol. = 1.2 mg/L) as well as $CaSO_3$ x H_2O (sol. = 70 mg/L), whereas H_2S gas may form [51] and dissipate within the cathodic open atmosphere. H_2S production at the anode (sulphur dropped from 24.7 to 20.9 mg/L) was confirmed by olfactory observations of the off-gas and the presence of desulfurization type bacteria (*Sec. 4.4.3.3*).

When considering flow rates of both wastewater (20 L/h) and groundwater (2.0 L/h), an elimination and recovery rate could be established. The elimination rate referred to the species reduction in the wastewater anolyte ($q_{Calcium}$ = 40 mg/h, $q_{Potassium}$ = 50 mg/h, $q_{Magnesium}$ = 2.0 mg/h, q_{Sodium} = 110 mg/h and $q_{Sulphur}$ = 75 mg/h), whereas the recovery rate was related to the species accumulation in the groundwater catholyte ($q_{Potassium}$ = 20 mg/h and q_{Sodium} = 70 mg/h).

3.4.2 N-Species / Denitrification

Experimental tests relative to nitrogen compounds (ammonium, nitrate and nitrite) suggested that denitrification occurred within the 1000-L MFC installation. Looking at the results of the analysis performed (*Sec. 3.10*) at the inlet and outlet of the MFC, for both anolyte and catholyte, it appeared that the total amount of N-species decreased when passing through the installation. The total nitrogen species flow rate dropped from 31.9 to 16.3 mmol/h (*Tab.14*), indicating a denitrification yield of 48.8%.

Parameters	*Anolyte$_{in}$*	*Anolyte$_{out}$*	*Catholyte$_{in}$*	*Catholyte$_{out}$*	***Legislation [35]***
NH_4^+ [mg/L]	*28.7*	*13.9*	*0.03*	*0.05*	***2.0***
NO_3^- [mg/L]	*0.09*	*0.07*	*0.81*	*29.0*	***N/A***
NO_2^- [mg/L]	*0.03*	*0.02*	*0.01*	*0.01*	***0.3***
Total N-species [mmol/h]	***31.9***	***15.4***	***0.03***	***0.94***	

Table 11: *Nitrogen species (NH_4^+, NO_3^- & NO_2^-) concentrations and flow rates at the inlet and outlet of the 1000-L MFC for both anolyte and catholyte. The experimental conditions were the following: q_{an} = 20 L/h, q_{cat} = 2.0 L/h with P_{air} = 0.5 bar and MPPT device as storing modules.*

N-species (especially NH_4^+) are abundant in WWTP and naturally found in large amounts (28.7 mg/L) in the anodic compartments of the 1000-L MFC (*Tab.14*). The detected concentration of nitrate (NO_3^-) was higher in groundwater (0.81 mg/L) than wastewater (0.09 mg/L). Ammonium (NH_4^+) could have migrated through the proton exchange membrane (extrapolation estimated a NH_4^+ migration between 5 to 20%), from the anodic compartment, to compensate the accumulation of negative charges at the cathode (*Sec. 2.2*).

Two pathways of denitrification were possible. A stripping phenomenon was conceivable in the cathodic compartment of the MFC. At the operating catholyte pH (7.3-8.4), the speciation of NH_4^+/ NH_3 favour the ammonium form [52]. However, a small fraction of the ammonium migrating should be found under the form of ammoniac gas (NH_3) and be stripped out of the cell by the constant air bubbling supplying oxygen to the catholyte. The second possibility was related to the electrochemical reduction of nitrogen compounds into N_2 gas (*Eqs.18*). These reactions could occur in both compartments since denitrifying bacteria were found in either of them (*Sec. 4.4.3.3, Fig.55*).

$$2NO_3^- + 10e^- + 12H^+ \rightarrow N_2 \uparrow + 6H_2O \qquad (18a)$$

$$2NO_2^- + 6e^- + 8H^+ \rightarrow N_2 \uparrow + 4H_2O \qquad (18b)$$

$$2NH_4^+ + 3O_2 + 6e^- + 4H^+ \rightarrow N_2 \uparrow + 6H_2O \qquad (18c)$$

3.4.3 Micropollutants Analysis

The micropollutants that need to be treated are mostly issued from the pharmaceutical industry and could be classified in two distinct categories: the compounds very easily eliminated (category 1) and the molecules easily eliminated (category 2). The list of recommended treatable micropollutants is the following:

Category 1: Amisulpride (antidepressant), Carbamazepine (anticonvulsant), Citalopram (antidepressant), Clarithromycin (antibiotic), Diclofenac (anti-inflammatory), Hydrochlorothiazide (diuretic), Metoprolol (beta blocker) and Venlafaxine (antidepressant).

Category 2: Benzotriazole (anti-corrosion), Candesartan (antihypertensive), Irbesartan (antihypertensive) and Methylbenzotriazole (anti-corrosion).

Samples were collected at the inlet and outlet of the MFC installation. The outlet sample was taken after 23.4 h, corresponding to the residence time for wastewater treatment lines. An average micropollutants elimination yield of 64.9% was observed (*Fig.60B*), in comparison to the recommended Swiss legal basis value of 80% [53]. The analysis was conducted just once and needs more work, it was with 15% below the legislators requirement considered not impossible to achieve 80% once the setup's performance becomes enhanced.

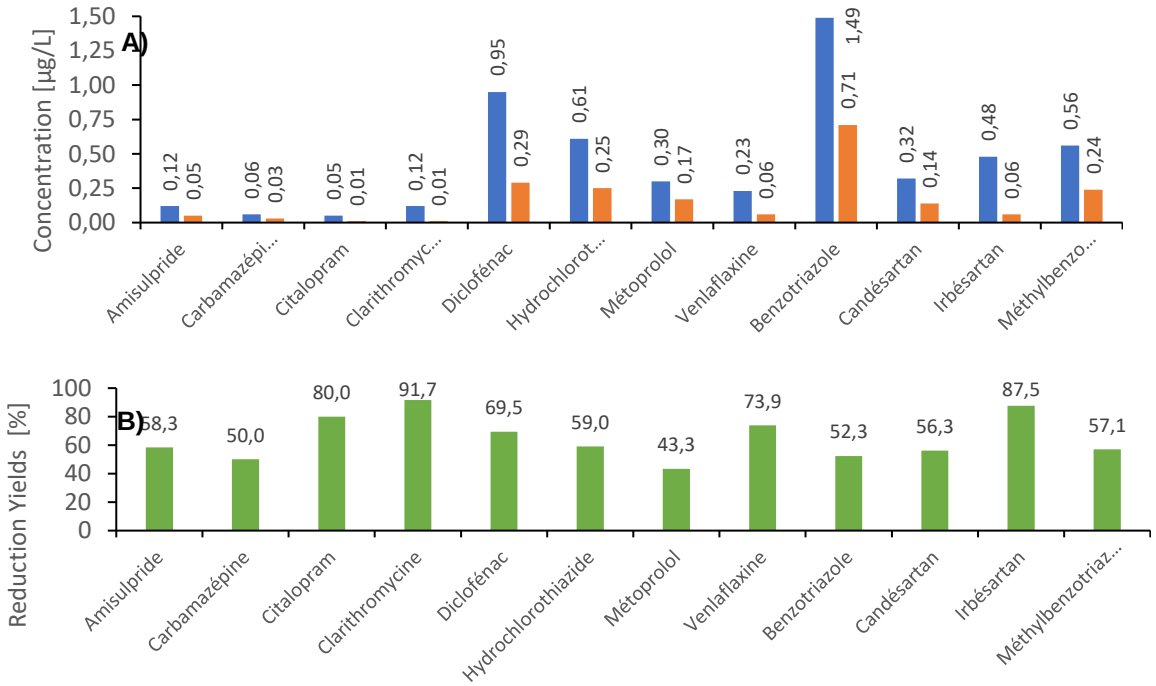

Figure 43: *Micropollutants concentration at the inlet and outlet of the of the 1000 L-MFC installation (**A**) as well as corresponding reduction yields (**B**).*

3.5 Methane Production from Precipitated Organic Mass

A qualitative gas analysis was performed in the headspaces of the first microbial fuel cells of each treatment line (*Fig.13*) to determine if any particular gaseous molecules were formed. Methane (CH_4) and carbon dioxide (CO_2) were found by micro GC analyses (*Fig.61*). When comparing the area of the obtained pics for each chromatogram to a reference standard (*Sec. 8.3J*), it was possible to determine the proportion of each gas present within the MFCs headspaces (*Tab.15*). All chromatograms are found in the appendix (*Sec. 8.3J*).

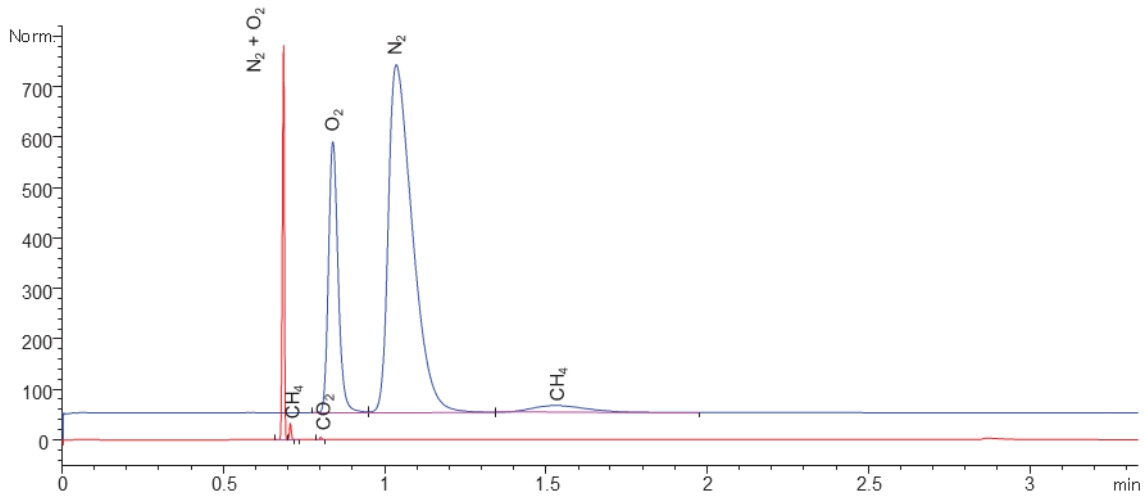

Figure 44: *Gas quantification (1.1c) chromatograms. The MS5A column (blue line) permitted to determine the concentration of H_2 (0.631 min), O_2 (0.840 min), N_2 (1.037 min) and CH_4 (1.529 min), whereas the PPU column (red line) allowed quantifying air (O_2 + N_2)(0.688 min), CH_4 (0.709 min) and CO_2 (0.803 min).*

An average of 0.81% of methane was present in the first microbial fuel cell, whereas a concentration of 0.69% of carbon dioxide was found (*Tab.15*). CO_2 came from the degradation (oxidation) of organic matter by anaerobic microorganisms (*Fig.2*), while CH_4 was generated as the metabolic by-product of methanogens. Thus, the average biogas produced from these MFCs had the following composition (CH_4 : CO_2) ratio: 54.0 : 46.0.

Gas [%]	*Blanc*	*1.1a*	*1.1b*	*1.1c*	*1.1d*	***Average***
CH_4	< 0.02	0.23	1.10	1.52	0.38	**0.81**
CO_2	< 0.12	0.44	0.78	1.09	0.44	**0.69**
Air	> 99.86	99.33	98.12	97.39	99.18	**98.50**

Table 12: *Proportion of methane and carbon dioxide within the headspace of four MFCs (Fig.13). The percentage of each species was deduced from the area of each pic when comparing to a reference standard.*

The methane production rate of a MFC ($C\dot{H}_{4_{Reactor}}$ $[ml/day]$) could be calculated by knowing the headspace concentration of each gas ($CH_4[\%]$ and $CO_2[\%]$), the total headspace capacity ($V_{headspace} = 1.95\ [L]$) as well as the process time ($t = 190\ [h]$). When considering one microbial fuel cell, the equation was described as follows (*Eq.19*):

$$C\dot{H}_{4_{Reactor}} = \frac{CH_4}{100} \cdot \frac{24}{t} \cdot 1000\, V_{headspace} \qquad (19)$$

Methane (CH_4) formation in a microbial fuel cell installation limits the production of bioelectricity because the electrons generated by the oxidation of the organic matter could be employed during methanogenesis and produced reduced metabolites such as methane or hydrogen gas [54]. Therefore, the presence of CH_4 needs to be avoided in order to maintain the MFC performance to the maximum. Fortunately, only in the first MFC was a notable quantity of methane detected (*Fig.13, 1.1 a-d*). In the following reactors (*Fig.13, 1.2 a-d*), only trace of methane were observed (*Tab.16*). The difference between the first and second cell was the accumulation of organic matter. Visually, the organic mass found at the bottom of the first reactor was more important than the one observed in the second treatment cell, which tended to indicate that methane production was affected by the presence of solid organic matter in the anolyte. To support that claim, the methane generated in the first MFC was controlled again but after having the cell purged with fresh anolyte, removing the precipitate organic mass. In that situation, the methane production dropped from 2.00 to 0.07 mL/day, representing a reduction of approximatively 96.5%.

Configurations / Parameters	*Ratio CH_4/CO_2 [%]*	*CH_4 headspace [%]*	*CH_4 [mL/day]*
A) First MFC Reactor	54.0 : 46.0	0.81	2.00
B) Second MFC Reactor	5.3 : 94.7	0.01	0.02
C) First MFC Reactor after Purge	6.6 : 93.4	0.03	0.07

Table 13: *Biogas ratio, as well as headspace methane concentrations and production rates under different configurations.*

To optimise the system, the precipitate organic matter needs to be removed and delivered to a digester where it will be converted into methane without impacting the energy generated with the 1000-L MFC installation.

The results relative to the gas analysis of the second row of MFC reactors as well as the first row of MFC reactors after purging conditions were summarised under the form of tables and displayed in the appendix section (*Sec. 8.3J*).

3.6 Possible Electron Sink Sources

The probable electron sink could be diverse and varied. The main reasons are listed on the following table (*Tab.17*). Because wastewater entering the 1000-L MFC always contained dissolved oxygen (*Sec. 4.1.1*), some electrons generated by the microbial oxidation of the organic matter would be drawn toward the oxygen instead of passing through the electrical circuit and producing energy. As showed in the metagenomics analysis (*Sec. 4.4.3.3*), denitrifying type bacteria were present in the system and may use electrons for the denitrification of N-species (*Sec. 4.5.2*). The same problematic might occur with sulphate type bacteria that should reduce S-compounds present in wastewater (*Sec. 4.5.1*). Methane production was a reality under certain circumstances for the first cell of each treatment line (*Sec. 4.6*) and the formation of CH_4 molecules reduced the electronic flux from anode to cathode. Some microorganisms could also utilise electrons during their metabolism, especially towards biomass formation. Finally, ferric iron (*Sec. 4.5.1*), employed as precipitation agent to eliminate phosphate, may be reduced by electrons liberated by exoelectrogens species. This might also be valid for other metallic compounds present in wastewater, such as heavy metals. To reduce the impact of electron sinks further down is to control the oxygen in the anode. Such an approach is possible by automation in controlling the injection of air-oxygen in the cathode. The other important sink is methane generation and here sludge has to be removed. The current reactor design is in this respect not well designed.

Causes :	Chemical Equations :
A. Residual Oxygen	$O_2 + 4H^+ + \mathbf{4}e^- \rightarrow 2H_2$
B. Denitrification	$NO_3^- + 2H^+ + \mathbf{2}e^- \rightarrow NO_2^- + 2H_2O$ $NO_2^- + 2H^+ + e^- \rightarrow NO + H_2O$
C. Sulphate / Sulphite Reduction	$SO_4^{2-} + 2H^+ + \mathbf{2}e^- \rightarrow SO_3^{2-} + H_2O$ $SO_3^{2-} + 8H^+ + \mathbf{6}e^- \rightarrow H_2S + 3H_2O$
D. Methane Production	$CO_2 + 8H^+ + \mathbf{8}e^- \rightarrow CH_4 + 2H_2O$
E. Biomass Formation	$HCO_3^- + 5H^+ + \mathbf{4}e^- \rightarrow CH_2O + 2H_2O$
F. Iron Reduction	$Fe^{3+} + e^- \rightarrow Fe^{2+}$
G. Other Metal Reduction	$M^{x+} + \mathbf{y}e^- \rightarrow M^{(x-y)}$

Table 14: *Probable causes inducing electron sink in the MFC installation with their corresponding chemical equations.*

3.7 Potential Energy Savings

3.7.1 Oxygen and Air Requirements

Theoretically, the requirements relative to oxygen is similar whereas biological lagoon treatment or microbial fuel cell technology are involved. If glucose ($C_6H_{12}O_6$) is considered as typical organic matter, one mole of glucose required 6 moles of oxygen to be transformed into CO_2 and water (*Eqs.20*).

Glucose transformation for typical biological treatment (aerobic conditions):

$$C_6H_{12}O_6 + 6O_2 \rightarrow 6CO_2 + 6H_2O \qquad (20a)$$

Glucose transformation with microbial fuel cell technology (anaerobic conditions):

$$Anodic\ Reaction\colon\ C_6H_{12}O_6 + 6H_2O \rightarrow 6CO_2 + 24H^+ + 24e^- \qquad (20b)$$

$$Cathodic\ Reaction\colon\ 6O_2 + 24H^+ + 24e^- \rightarrow 12H_2O \qquad (20c)$$

$$Overall\ Reaction\colon\ C_6H_{12}O_6 + 6O_2 \rightarrow 6CO_2 + 6H_2O \qquad (20d)$$

The oxygen required from both processes is related to the organic matter present in wastewater and measured by the chemical oxygen demand (COD). The average COD removed in Châteauneuf WWTP during part of the project duration (01.10.18 to 01.10.19) was 325 mg/L indicating that in order to treat one litre of wastewater, 0.325 g of O_2 was needed. Knowing the daily treatment rate (17'500 m^3/day), it was possible to calculate (*Eq.16, Sec. 3.11*) the oxygen consumption per day and year: 5'690 kg/day or 2'075 ton/year.

The minimal air requirements could be approximate using *equation 17 (Sec. 3.11)*. A minimal daily air consumption of 19'000 m^3 was estimated, corresponding to an annual volume of approximatively 7 million cubic meters of air. These figures correspond to an ideal case scenario were all the molecules of oxygen present in the air are transferred to wastewater. However, in reality only a fraction of oxygen is transferred from the gas to the liquid phase (mass transfer), which increases the air requirement by at least a factor 10. The large amount of air needed, requires the use of powerful blowers in order to supply oxygen to wastewater. The electricity consumption of the *Châteauneuf* WWTP was 0.73 GWh/year, corresponding to an annual cost of 100'000 CHF.

At the MFC scale when considering a treatment rate of one cubic meter per day, an amount of 325 g of oxygen was required, corresponding to a daily minimal volume of 1.09 m^3 of air. With a mass transfer of 10%, the volume of air increases to 10.9 m^3/day.

3.7.2 Possible Savings Solutions with MFC Technology

In order to reduce the air consumption of the 1000-L MFC, several solutions could be implemented. For instance:

A) Adapt the air bubbling to favour higher mass transfer. However, in this case, blowers are still required because the theoretical minimal amount of air needed remains the same (7 million m^3 per year), but the part of oxygen transferred from gaseous to liquid phase is more important and thus, the air requirement lower than the 70 million m^3/year as estimated for Châteauneuf WWTP.

B) Use a water source that is naturally oxygenated such as a river as catholyte. For example, if considering the river *Sionne*, 8.66 mg/L of oxygen was detected in solution. To sustain the oxygen consumption during the actual MFC process where 1 m^3 of wastewater is treated per day, a flow rate of 1.56 m^3/h needs to be supplied to the installation. This solution is conceivable for small and/or medium installations. However, when large wastewater treatment plants are considered, the amount of oxygenated water would be much more consequent. As an example, *Châteauneuf* WWTP would require a flowrate of 7.6 m^3/s.

C) Take advantage of the N-species present in the catholyte that can also accept electrons and replace some of the needed oxygen. The benefit of N-species is the fact that they are present in abundant quantity in wastewater under the form of ammonium (NH_4^-) and, thus, no additional energy should be required such as air bubbling. (*Sec. 4.1.1*).

D) Introduce algae at the cathodic compartment. They will consume carbon dioxide (CO_2) generated in the anodic chamber and produce oxygen through photosynthesis (*Eq.21*). This is a self-sufficient system that does not require external energy input.

$$Anodic\ Reaction: C_6H_{12}O_6 + 6H_2O \rightarrow 6CO_2 + 24H^+ + 24e^- \qquad (20b)$$

$$Photosynthesis: 6CO_2 + 12H_2O \xrightarrow{Light} C_6H_{12}O_6 + 6O_2 + 6H_2O \qquad (21)$$

$$Cathodic\ Reaction: 6O_2 + 24H^+ + 24e^- \rightarrow 12H_2O \qquad (20c)$$

E) Implement the system with air cathodes where oxygen will be directly consumed at the electrode interface from air without any additional energy requirements. However, the problematic here is that a precipitate will form on the electrode surface reducing the process efficiency over time. The air-cathodes, thus, need periodical precipitate removal to keep the process running in the best possible conditions. Moreover, with air-cathodes O_2 could easily pass through the membrane in the anolyte and a biofilm might develop directly on the membrane anodic side, increasing the internal resistance of the system.

3.8 Comparison of our MFC with International Large Scale MFCs (>10L)

Comparing MFC performances from wastewater treatment was difficult due to the multitude of MFC-designs as well as wastewater compositions. Nevertheless, there are some key parameters to assess each MFC-system in terms of water purification performance and energy production. The COD removal allowed determining the charge of organic pollutant eliminated from the water passing through the installation. The energy per cubic meter is an interesting parameter that can be employed to roughly estimate the energy production at the scale of a given WWTP. Here, wastewater composition constantly changed and it made more sense to compare the system in terms of energy generated as a function of COD removal. Coulombic and energy efficiency are two parameters used to evaluate MFCs for electrical performances in terms of current (CE) generated and energy (EE) produced. Results of eight recent studies were compared with the 1000 L-MFC installation (*Tab.18*):

[References] (Year)	Wastewater Type	Capacity Total [L]	Energy Density [kWh/m³]	Energy Density [kWh/kg COD]	COD Removal [%]	Coulombic Efficiency [%]	Energy Efficiency [%]
[43,55] (2011)	Domestic	20	0.004	0.011	66 - 80	0.30	0.28
[56] (2012)	Brewery	10	0.200 [a]	0.109 [a]	87.1	6.3 - 7.6	2.8
[43,57] (2014)	Domestic	250	0.054	0.206	79	3 - 7	5.3
[58] (2015)	Brewery	90	0.056 - 0.097	0.033	82.7 – 86.5	8.0 - 19.1	0.85
[43] (2016)	Clarifier	45	0.007 – 0.025	0.360	13.5 - 67.0	10.1 - 24.8	9.3
[59] (2016)	Synthetic	72	0.071-0.131 [b]	0.194 - 0.473 [b]	78 - 97	1 - 14	5.0 - 12.3
[60] (2017)	Brewery	20	0.030-0.310	0.033-0.359	47.6 - 94.5	5.5 - 53.6	0.85 - 9.3
[61] (2018)	Domestic	1000	0.015 [c]	0.242 [c]	70 - 80	41 - 75	6.3
This study	***Clarifier***	***925-1030***	***0.006 - 0.060***	***0.224 - 0.469***	***34.4 – 95.4***	***4.7 – 14.9***	***5.8 – 12.1***

Table 15: *Performance comparison of up-scale MFCs (> 10 L). Incomplete data were added based on calculations from values (power densities, COD removal rates and concentration of COD removed) found in the cited literature: a) 4.1 W/m³; 0.9 kg COD/m³d; 1.825 kg COD/m³. b) 25.6 – 42.1 W/m³; 1.3 - 5.2 kg COD/m³d; 0.15 – 0.675 kg COD/m³. c) 7.5 W/m³; 0.031 kg COD/m³h; 63.5 g COD/m³.*

Wastewater treatment using lab-scale MFC technology was already established since quite some time and large-scale installations confirmed that trend. By adjusting the HRT of the system, it was possible to reach the minimal requirement for wastewater disposal [35] and even achieved COD removal efficiencies up to 95% (*Tab.18*). The energy harvested per kg of COD increased with systems evolution and better comprehension in the MFC field. From 2011 to 2015 the energy generated was comprised between 0.01 and 0.20 kWh per kg of COD removed. In the last 3 years it ranged from 0.20 to 0.47 kWh/kg COD due to improved energy efficient installations: [5.0, 12.3%] against [0.28, 5.3%] before 2016. The proposed 1000-L MFC installation followed this trend with the best results in terms of energy efficiency (12.1%) for the use of municipal wastewater (*Tab.18*), an increase of 43x comparing to 2011.

4 Conclusion

The implementation of the 1000-L MFC as pilot directly within the WWTP of *Châteauneuf* permitted to treat wastewater in accordance to the Swiss legislation (COD < 60 mg/L; removal rate > 80%) up to a capacity of 1 m^3/day. Under these considerations, the process effectiveness reached up to 4.7% for Coulombic efficiency as well as 5.8% for Energy efficiency. When working at lower flow rates the efficiencies could even reached 14.9 and 12.1%, respectively. These results were on the good side when comparing to similar international studies, particularly due to the implementation of MPPT devices that boosted the energy storage on lithium batteries.

The energy recovered from the process varied between 0.006 and 0.060 kWh/m^3, which corresponded to 0.22 - 0.47 kilowatt-hours generated per kilogram of COD removed. An average annual power of 172 mW (max. 650 mW) corresponding to 1.51 kWh of energy was generated during year 2019. The energy produced by the installation increased though time due to microorganisms' growth and biofilm maturation. An augmentation of factor 7 was found within a half year of utilisation. The power generated by the installation was also affected by day & night cycles as well as weather conditions and seasonal occurrences, especially during the grape harvest period where higher internal resistances were noticed.

Voltage reversal (inversion of the potential of a cell) negatively impact (-8.6%) on energy production because, even though, the majority of the treatment lines (10 out of 16) were performing as expected, 4 cart-lines worked with medium reduced efficiencies and 2 additional lines were highly impacted by inversions. Electron sinks could be one possible cause of voltage reversal. The probable sources of electron sinks in the anolyte are multiple: presence of residual oxygen, denitrification, sulphate / sulphite reduction, methane production, biomass formation or even metal reduction such as ferric iron.

Dissolved oxygen increased the power output of the MFC by a factor 5.7x. However, compressed air bubbling is an energy-consuming process. The potential energy savings in terms of oxygen / air consumption was not quantifiable due to lack of data. However, the minimal air consumption for *Châteauneuf* WWTP was estimated at 7 million cubic meter per year. The annual energy investment of the treatment plant was close to 0.73 GWh for a total cost of 100'000 CHF. Several solutions could be implemented in order to reduce the total air consumption. Among these proposed methods are the use of an alternative oxygenated water source, the introduction of algae in the cathodic compartment of the MFC or the implementation of air-cathodes to the actual system.

DNA microorganism concentrations were higher at the outlet of the installation, whereas operational taxonomic units (OTU) were more important at the entrance, suggesting that the microbiome was more diverse at the system inlet, while it became less varied but more developed / matured at the outlet. Metagenomic data demonstrated a dominance of exoelectrogens species in the first MFC cart, mostly composed by Geobacter species (> 80%) and a presence of nitrification / denitrification type bacteria in the whole installation.

Experiments suggested that denitrification occurred with the 1000-L MFC with yields up to 48.8%. Moreover, a micropollutant treatment was observed with an average elimination yield of 64.9% The formation of methane was limited to the first cell of each treatment line and explained by the accumulation of organic matter in these anodic compartments. Cells purge reduced the methane formation by 96.5%, preventing power drop generation related to electrons flow disruption.

The treated effluents could be released into the environment because the phosphate (PO_4^{3-}) concentration (0.59 mg/L) at the system output was within the legislation (< 0.8mg/L) and no heavy metal were detected, except Ni (0.60 mg/L) and Zn (0.09 mg/L) but in low concentrations. Wastewater was depleted in calcium (40 mg/h) potassium (50 mg/h), sodium (110 mg/h) and sulphur (75 mg/h) due to migration flows, naturally occurring in each MFC reactor from anode to cathode. The groundwater, on the other hand, was enriched in potassium (20 mg/h) and sodium (70 mg/h).

5 Future Perspectives

The principles of the microbial fuel cell technology allowed wastewater treatment while generating energy. It might be, in a foreseeable future, directly implemented in WWTPs as substitute / complement to biological lagoons due to the potential lower operating costs (neutral energy balance possible if implemented with energy savings methods). However, the actual technology only permits to treat small capacities (up to 1 m^3/day) in regard to the daily volume of wastewater that needs to be treated (17'500 m^3/day for *Châteauneuf* WWTP). Currently, the MFC volume needed to accommodate *Châteauneuf* WWTP treatment capacity corresponds to 18'000 m^3, which corresponds to the surface of a soccer filed (7000 m^2) when the MFC reactors are stacked to a 2.5 m height. The oncoming challenge is, thus, to be able to transpose the current MFC technology to large treatment scales. Alternative sizing perspectives (design modification) and costs optimisations (material substitution) need to be consdered in this regard.

6 Bibliography

1. Longo, S.; d'Antoni, B. M.; Bongards, M.; Chaparro, A.; Cronrath, A.; Fatone, F.; Lema, J. M.; Mauricio-Iglesias, M.; Soares, A.; Hospido, A., Monitoring and diagnosis of energy consumption in wastewater treatment plants. A state of the art and proposals for improvement. *Applied Energy* **2016,** *179*, 1251-1268.
2. Metcalf; Eddy, *Wastewater Engineering: Treatment and Reuse*. 4th ed.; McGraw-Hill: New York, 2006.
3. Elias-Maxil, J. A.; van der Hoek, J. P.; Hofman, J.; Rietveld, L., Energy in the urban water cycle: Actions to reduce the total expenditure of fossil fuels with emphasis on heat reclamation from urban water. *Renewable & Sustainable Energy Reviews* **2014,** *30*, 808-820.
4. Venkatesh, G.; Brattebo, H., Energy consumption, costs and environmental impacts for urban water cycle services: Case study of Oslo (Norway). *Energy* **2011,** *36* (2), 792-800.
5. Gikas, P., Towards energy positive wastewater treatment plants. *Journal of Environmental Management* **2017,** *203*, 621-629.
6. Liu, H.; Ramnarayanan, R.; Logan, B. E., Production of electricity during wastewater treatment using a single chamber microbial fuel cell. *Environmental Science & Technology* **2004,** *38* (7), 2281-2285.
7. Wakeel, M.; Chen, B.; Hayat, T.; Alsaedi, A.; Ahmad, B., Energy consumption for water use cycles in different countries: A review. *Applied Energy* **2016,** *178*, 868-885.
8. Barroso Soares, R.; Santos Memelli, M.; Pereira Roque, R.; Franci Gonçalves, R., Comparative Analysis of the Energy Consumption of Different Wastewater Treatment Plants. *International Journal of Architecture, Arts and Applications* **2017,** *3* (6), 79-86.
9. Huggins, T.; Fallgren, P.; Jin, S.; Ren, Z., Energy and Performance Comparison of Microbial Fuel Cell and Conventional Aeration Treating of Wastewater. *Microbial & Biochemical Technology* **2013,** *S6*, 2-5.
10. Shen, Y. W.; Linville, J. L.; Urgun-Demirtas, M.; Mintz, M. M.; Snyder, S. W., An overview of biogas production and utilization at full-scale wastewater treatment plants (WWTPs) in the United States: Challenges and opportunities towards energy-neutral WWTPs. *Renewable & Sustainable Energy Reviews* **2015,** *50*, 346-362.
11. Oh, S. T.; Kim, J. R.; Premier, G. C.; Lee, T. H.; Kim, C.; Sloan, W. T., Sustainable wastewater treatment: How might microbial fuel cells contribute. *Biotechnol Adv* **2010,** *28* (6), 871-881.
12. Li, W. W.; Yu, H. Q.; He, Z., Towards sustainable wastewater treatment by using microbial fuel cells-centered technologies. *Energ Environ Sci* **2014,** *7* (3), 911-924.
13. Zhang, F.; Ge, Z.; Grimaud, J.; Hurst, J.; He, Z., Long-Term Performance of Liter-Scale Microbial Fuel Cells Treating Primary Effluent Installed in a Municipal Wastewater Treatment Facility. *Environmental Science & Technology* **2013,** *47* (9), 4941-4948.
14. Asai, Y.; Miyahara, M.; Kouzuma, A.; Watanabe, K., Comparative evaluation of wastewater-treatment microbial fuel cells in terms of organics removal, waste-sludge production, and electricity generation. *Bioresour Bioprocess* **2017,** *4*.
15. Zhang, F.; Ge, Z.; Grimaud, J.; Hurst, J.; He, Z., In situ investigation of tubular microbial fuel cells deployed in an aeration tank at a municipal wastewater treatment plant. *Bioresource Technology* **2013,** *136*, 316-321.
16. Arredondo, M. R.; Kuntke, P.; Jeremiasse, A. W.; Sleutels, T. H. J. A.; Buisman, C. J. N.; ter Heijne, A., Bioelectrochemical systems for nitrogen removal and recovery from wastewater. *Environmental Science-Water Research & Technology* **2015,** *1* (1), 22-33.
17. Cucu, A.; Tiliakos, A.; Tanase, I.; Serban, C. E.; Stamatin, I.; Ciocanea, A.; Nichita, C., Microbial Fuel Cell for Nitrate Reduction. *Eenviro-Yrc 2015 - Bucharest* **2016,** *85*, 156-161.
18. The Swiss Federal Office of Energy, Production and consumption of energy in Switzerland. 2018.
19. Pandit, S.; Das, D., Principles of Microbial Fuel Cell for the Power Generation. In *Microbial Fuel Cell: A Bioelectrochemical System that Converts Waste to Watts*, Das, D., Ed. Springer International Publishing: Cham, 2018; pp 21-41.
20. Modin, O.; Gustavsson, D. J. I., Opportunities for microbial electrochemistry in municipal wastewater treatment - an overview. *Water Science and Technology* **2014,** *69* (7), 1359-1372.
21. Das, D.; Varanasi, J. L., Fundamentals of biofuel production processes. Taylor & Francis, CRC Press,: Boca Raton, 2019; p. 1 online resource.

22. Logan, B. E.; Hamelers, B.; Rozendal, R. A.; Schrorder, U.; Keller, J.; Freguia, S.; Aelterman, P.; Verstraete, W.; Rabaey, K., Microbial fuel cells: Methodology and technology. *Environmental Science & Technology* **2006,** *40* (17), 5181-5192.
23. Ucar, D.; Zhang, Y. F.; Angelidaki, I., An Overview of Electron Acceptors in Microbial Fuel Cells. *Frontiers in Microbiology* **2017,** *8*, 643.
24. He, Z., Development of Microbial Fuel Cells Needs To Go beyond "Power Density". *Acs Energy Letters* **2017,** *2* (3), 700-702.
25. McCarty, P. L.; Bae, J.; Kim, J., Domestic Wastewater Treatment as a Net Energy Producer-Can This be Achieved? *Environmental Science & Technology* **2011,** *45* (17), 7100-7106.
26. Scherson, Y. D.; Criddle, C. S., Recovery of Freshwater from Wastewater: Upgrading Process Configurations To Maximize Energy Recovery and Minimize Residuals. *Environmental Science & Technology* **2014,** *48* (15), 8420-8432.
27. Xiandeng, H.; Bradley, T. J., Inductively Coupled Plasma/Optical Emission Spectrometry. In *Encyclopedia of Analytical Chemistry*, R.A. Meyers ed.; John Wiley & Sons Ltd: Chichester, 2000; pp 9468–9485.
28. Siva Sai Kiran, B.; Raja, S., A Review on Inductively Coupled Plasma Optical Emission Spectrometry (Icp-Oes) with a Special Emphasis on its Applications. *Der Pharmacia Lettre* **2017,** *9*, 44-54.
29. Bolleter, W. T.; Bushman, C. J.; Tidwell, P. W., Spectrophotometric Determination of Ammonia as Indophenol. *Analytical Chemistry* **1961,** *33* (4), 592-&.
30. Hartley, A. M.; Asai, R. I., Spectrophotometric Determination of Nitrate with 2,6-Xylenol Reagent. *Analytical Chemistry* **1963,** *35* (9), 1207-&.
31. Virdis, B.; Rabaey, K.; Rozendal, R. A.; Yuan, Z. G.; Keller, J., Simultaneous nitrification, denitrification and carbon removal in microbial fuel cells. *Water Research* **2010,** *44* (9), 2970-2980.
32. Kim, K. Y.; Yang, W. L.; Logan, B. E., Impact of electrode configurations on retention time and domestic wastewater treatment efficiency using microbial fuel cells. *Water Research* **2015,** *80*, 41-46.
33. Oliveira, V.; Carvalho, T.; Melo, L.; Pinto, A.; Simoes, M., Effects of Hydrodynamic Stress and Feed Rate on the Performance of a Microbial Fuel Cell. *Environmental Engineering and Management Journal* **2016,** *15* (11), 2497-2504.
34. Freguia, S.; Rabaey, K.; Yuan, Z. G.; Keller, J., Electron and carbon balances in microbial fuel cells reveal temporary bacterial storage behavior during electricity generation. *Environmental Science & Technology* **2007,** *41* (8), 2915-2921.
35. The Swiss Confederation, Water Protection Ordinance (814.201) of 28 October 1998 (Status as June 2018) , Art.6, Annex 3.2. 2018.
36. Etat de Fribourg, Définition et calculs des équivalent-habitants (Notice d'information 4.2.024). 2017.
37. Aghababaie, M.; Farhadian, M.; Jeihanipour, A.; Biria, D., Effective factors on the performance of microbial fuel cells in wastewater treatment – a review. *Environmental Technology Reviews* **2015,** *4* (1), 71-89.
38. Tang, J. H.; Liu, T.; Yuan, Y.; Zhuang, L., Effective Control of Bioelectricity Generation from a Microbial Fuel Cell by Logical Combinations of pH and Temperature. *Scientific World Journal* **2014,** *2014*, 186016.
39. Tremouli, A.; Martinos, M.; Lyberatos, G., The Effects of Salinity, pH and Temperature on the Performance of a Microbial Fuel Cell. *Waste and Biomass Valorization* **2017,** *8* (6), 2037-2043.
40. Dijkstra, P.; Thomas, S. C.; Heinrich, P. L.; Koch, G. W.; Schwartz, E.; Hungate, B. A., Effect of temperature on metabolic activity of intact microbial communities: Evidence for altered metabolic pathway activity but not for increased maintenance respiration and reduced carbon use efficiency. *Soil Biology & Biochemistry* **2011,** *43* (10), 2023-2031.
41. Larrosa-Guerrero, A.; Scott, K.; Head, I. M.; Mateo, F.; Ginesta, A.; Godinez, C., Effect of temperature on the performance of microbial fuel cells. *Fuel* **2010,** *89* (12), 3985-3994.
42. Li, J. H.; Lu, X. W., Effect of Seasonal Temperature on the Performance and on the Microbial Community of a Novel AWFR for Decentralized Domestic Wastewater Pretreatment. *Applied Sciences-Basel* **2017,** *7* (6).
43. Hiegemann, H.; Herzer, D.; Nettmann, E.; Lubken, M.; Schulte, P.; Schmelz, K. G.; Gredigk-Hoffmann, S.; Wichern, M., An integrated 45 L pilot microbial fuel cell system at a full-scale wastewater treatment plant. *Bioresource Technology* **2016,** *218*, 115-122.

44. Li, L. H.; Sun, Y. M.; Yuan, Z. H.; Kong, X. Y.; Li, Y., Effect of temperature change on power generation of microbial fuel cell. *Environmental Technology* **2013,** *34* (13-14), 1929-1934.

45. Zhi, W.; Ge, Z.; He, Z.; Zhang, H. S., Methods for understanding microbial community structures and functions in microbial fuel cells: A review. *Bioresource Technology* **2014,** *171*, 461-468.

46. Mysara, M.; Vandamme, P.; Props, R.; Kerckhof, F. M.; Leys, N.; Boon, N.; Raes, J.; Monsieurs, P., Reconciliation between operational taxonomic units and species boundaries. *Fems Microbiol Ecol* **2017,** *93* (4).

47. Parsons, S.; Berry, T., Chemical phosphorus removal. In *Phosphorus in Environmental Technologies: Principles and Applications*, Valsami-Jones ed.; IWA Publishing: London, 2004; pp 260-271.

48. Smith, V. H.; Tilman, G. D.; Nekola, J. C., Eutrophication: impacts of excess nutrient inputs on freshwater, marine, and terrestrial ecosystems. *Environ Pollut* **1999,** *100* (1-3), 179-96.

49. Wilfert, P.; Kumar, P. S.; Korving, L.; Witkamp, G. J.; van Loosdrecht, M. C. M., The Relevance of Phosphorus and Iron Chemistry to the Recovery of Phosphorus from Wastewater: A Review. *Environmental Science & Technology* **2015,** *49* (16), 9400-9414.

50. Physical Constants of Inorganic Compounds. In *Handbook of Chemistry and Physics*, David R. Lide ed.; CRC Press: USA, 2005.

51. Baeshov, A.; Myrzabekov, B.; Makhanbetov, A.; Mishra, B.; Baigenzhenov, O.; Luganov, V., Electrochemical Method for Producing Valuable Sulfur Compounds from Waste Materials. *International Journal of Nonferrous Metallurgy* **2017,** *6*, 17-26.

52. Jiang, X. J.; Cheng, Z. H.; Ma, W.; Gao, Z. X.; Ma, X. H.; Wang, R., Removal of Ammonia from Wastewater by Natural Freezing Method. *Aer Adv Eng Res* **2015,** *22*, 174-177.

53. Direction de l'environnement industriel urbain et rural (DIREV), Etat de Vaud, Traitement des micropolluants dans les stations d'épuration vaudoise. 2016.

54. Rabaey, K.; Boon, N.; Siciliano, S. D.; Verhaege, M.; Verstraete, W., Biofuel Cells Select for Microbial Consortia That Self-Mediate Electron Transfer. *Applied and Environmental Microbiology* **2004,** *70* (9), 5373-5382.

55. Jiang, D. Q.; Curtis, M.; Troop, E.; Scheible, K.; McGrath, J.; Hu, B. X.; Suib, S.; Raymond, D.; Li, B. K., A pilot-scale study on utilizing multi-anode/cathode microbial fuel cells (MAC MFCs) to enhance the power production in wastewater treatment. *International Journal of Hydrogen Energy* **2011,** *36* (1), 876-884.

56. Zhuang, L.; Yuan, Y.; Wang, Y. Q.; Zhou, S. G., Long-term evaluation of a 10-liter serpentine-type microbial fuel cell stack treating brewery wastewater. *Bioresource Technology* **2012,** *123*, 406-412.

57. Feng, Y. J.; He, W. H.; Liu, J.; Wang, X.; Qu, Y. P.; Ren, N. Q., A horizontal plug flow and stackable pilot microbial fuel cell for municipal wastewater treatment. *Bioresource Technology* **2014,** *156*, 132-138.

58. Dong, Y.; Qu, Y. P.; He, W. H.; Du, Y.; Liu, J.; Han, X. Y.; Feng, Y. J., A 90-liter stackable baffled microbial fuel cell for brewery wastewater treatment based on energy self-sufficient mode. *Bioresource Technology* **2015,** *195*, 66-72.

59. Wu, S. J.; Li, H.; Zhou, X. C.; Liang, P.; Zhang, X. Y.; Jiang, Y.; Huang, X., A novel pilot-scale stacked microbial fuel cell for efficient electricity generation and wastewater treatment. *Water Research* **2016,** *98*, 396-403.

60. Lu, M. Q.; Chen, S.; Babanova, S.; Phadke, S.; Salvacion, M.; Mirhosseini, A.; Chan, S.; Carpenter, K.; Cortese, R.; Bretschger, O., Long-term performance of a 20-L continuous flow microbial fuel cell for treatment of brewery wastewater. *Journal of Power Sources* **2017,** *356*, 274-287.

61. Liang, P.; Duan, R.; Jiang, Y.; Zhang, X. Y.; Qiu, Y.; Huang, X., One-year operation of 1000-L modularized microbial fuel cell for municipal wastewater treatment. *Water Research* **2018,** *141*, 1-8.